TWO PHOTON LUMINESCENCE FROM QUANTUM DOTS USING BROAD AND NARROWBAND ULTRAFAST LASER PULSES

A Thesis

by

HARIBHASKAR BALASUBRAMANIAN

Submitted to the Office of Graduate Studies of
Texas A&M University
in partial fulfillment of the requirements for the degree of

MASTER OF SCIENCE

December 2007

Major Subject: Biomedical Engineering

TWO PHOTON LUMINESCENCE FROM QUANTUM DOTS USING BROAD AND NARROWBAND ULTRAFAST LASER PULSES

A Thesis

by

HARIBHASKAR BALASUBRAMANIAN

Submitted to the Office of Graduate Studies of
Texas A&M University
in partial fulfillment of the requirements for the degree of

MASTER OF SCIENCE

Approved by:

Chair of Committee,	Kenith Meissner
Committee Members,	Alvin T. Yeh
	Michael A. Bevan
Head of Department,	Gerard L. Coté

December 2007

Major Subject: Biomedical Engineering

ABSTRACT

Two Photon Luminescence from Quantum Dots Using Broad and Narrowband Ultrafast Laser Pulses. (December 2007)

Haribhaskar Balasubramanian, B.E, University of Mumbai

Chair of Advisory Committee: Dr. Kenith Meissner

Nonlinear optical microscopy (NLOM) offers many advantages when imaging intact biological samples. By using ultrafast lasers in the near infrared and two photon excitation (TPE), signal production is limited to the focal volume and provides an excellent means for rendering thin, microscopic images from within the sample. Exogenous fluorophores/lumiphores may be used as efficient contrast agents to tag specific targets and provide enhanced signal. The efficiency of the TPE process in these contrast agents is broadly assumed to vary inversely with the laser pulsewidth, τ.

In this work, we investigate the TPE efficiency of transform limited broadband (~133nm, ~10fs) and narrowband (~11nm, ~170fs) pulses in the generation of two-photon luminescence from semiconductor nanocrystals or quantum dots (QD's) both theoretically and experimentally. Compared to standard organic dyes, QD's possess a relatively broad, uniform spectral response that enables better use of the full bandwidth from the broadband laser.

Theoretical calculations including both degenerate and non-degenerate TPE indicate a rolloff from the $1/\tau$ behavior as the pulses' spectral bandwidth becomes broader than the absorption spectra of the QD's. Experimentally measured enhancement

in luminescence intensity while using a broadband pulse is compared with the simulated enhancement in two-photon luminescence.

A combination of increased understanding of the excitation processes in NLOM and proper selection of contrast agents will help in advancing the role of broadband ultrafast lasers in NLOM.

To my affectionate and motivating parents and sister for their priceless support and guidance throughout my life.

ACKNOWLEDGMENTS

I am grateful to my advisor, Dr. Kenith Meissner who has been a patient listener to all my problems and would like to express my sincere gratitude to him for the financial support and encouragement throughout this research. He gave me a lot of confidence and inspired me whenever I thought I did not make a wise decision to switch over to Biomedical Engineering from Power Systems Engineering. I would also like to thank my committee members, Dr. Alvin Yeh and Dr. Michael Bevan. My special thanks to Dr. Yeh and Adam Larson, for their timely help in getting this work done successfully. I am also thankful to Shuo Pang, who shared his understanding in optics with me and also helped me in every way that he could.

My parents never tried to limit my aspirations and always encouraged me. Their belief in me and their support beyond measure has been the greatest motivating factor for me in life. I am grateful to them for being with me whenever I needed them. Finally, I would like to thank my cousins for all the support that they offered to me throughout my stay here.

NOMENCLATURE

QD	Quantum Dot
CdSe	Cadmium Selenide
ZnS	Zinc Sulfide
TOPO	Trioctylphosphine oxide
MAA	Mercaptoacetic acid
PAA	Polyallylamine
PVSA	Polyvinylsulfonic acid
TPA	Two photon absorption
PES	Photoluminescence excitation spectra

TABLE OF CONTENTS

LIST OF FIGURES

FIGURE Page

INTRODUCTION

Quantum dots (QD's) are bright, photostable lumiphores that have a broad excitation spectrum and a narrow emission spectrum at wavelengths that are dependent on the size of the particle. QD's allow efficient multicolor imaging of biological samples and are especially useful for luminescent imaging in biological tissues, where signals can be buried by scattering. Multiphoton microscopy enables deep imaging in a variety of biological samples and produces less overall photobleaching than wide-field or confocal microscopy. For transform limited ultrafast laser pulses, there exists an inverse relationship between pulsewidth, τ, and the two photon transition probability. When comparing broadband and narrowband pulses with the same delivered average power, the peak intensity of a temporally shorter laser pulse will be higher compared to the longer pulse.

$$\text{Average power} = \text{Peak power} * \text{Repetition rate} * \text{Pulse width}$$

We characterize the emission spectra of solutions containing colloidal QD's using broadband and narrowband pulses. Luminescence spectra are first taken using the narrowband laser at numerous wavelengths and then using broadband laser. We then investigate the enhancement in luminescence both theoretically and experimentally.

This thesis follows the style of *Langmuir*.

The reduced average power required for a given peak power of temporally shorter pulses reduces the photodamage to surrounding tissue. In living tissues, this corresponds to a decrease in thermal and oxidative damage.

BACKGROUND

Band theory of solids

Colloidal quantum dots are semiconductor nanocrystals which have been used in a wide array of fields including biomedical imaging, electro-optical devices, and computer applications.[1-7] To get a better understanding of the physics behind quantum dots, one must understand the band theory of solids.

Energy band structures in solids

For any material, electrical conductivity is determined by the number of electrons available to take part in conduction. The arrangement of energy states and the way in which each energy state is occupied by electrons determines the number of electrons available for conduction. In bulk semiconductor material, electrons have an array of energies. Only two electrons can fit in any given level. A bulk semiconductor has continuous energy bands as the individual energy levels in the band are so close together that there is no significant energy difference between them. Between the energy bands there may exist an energy band gap in which electrons may not possess the energies in the gap. For a semiconductor or an insulator, the band gap between the outer most bands, the valance band and conduction band, is very important in determining material properties. The energy bands will be collectively filled according to Pauli's exclusion principle. The final filled band is called the valence band. The next higher band is called the conduction band.

Valance band

The valance band is the outermost filled/partially filled band. At 0 K, in semiconductors and insulators the valance band is always completely filled with electrons. As the temperature starts to rise or when the electrons are excited by light, they absorb the energy to leave a vacant position in the valance band and move to the conduction band. However, the provided energy must be greater than the band gap. Electrons in the valence band do not participate in the conduction process. When excited from the valance band, the electron leaves behind an empty state in an ensemble of electrons. This pseudo particle is called as a hole and has properties opposite to that of an electron. The hole can move about the crystal, and thus contribute to the conductivity of the material.

Conduction band

Insulators and semiconductors have an empty conduction band. When an electron gains energy which is greater than the band gap energy of the crystal, it jumps to the conduction band. The conductivity is increased as the electron is free to move in the conduction band becoming a carrier. High electrical conductivity comes from ease of scattering electrons with an applied electric field. The approximate lifetime of an electron in the conduction band is a very small fraction of a second before the electron falls back to the valance band. When the electron loses its energy, it decays back to the valance band emitting energy in the form of heat and/or light which is called as photoluminescence emission. In semiconductors, the gap between valance and conduction band is small and energy in the form of heat or light will bridge the gap

making it possible for the electrons to move freely.[8] The energy bands in different types of materials are shown in figure 1.

The band gap determines the wavelength of light required to excite the electrons to the conduction band and also determines the emission wavelength of the light when the electron decays back to the valance band. The electron that decays back recombines with a hole. As the band gap is constant for a particular bulk material at a given temperature, the absorption and emission spectra are also constant.[9]

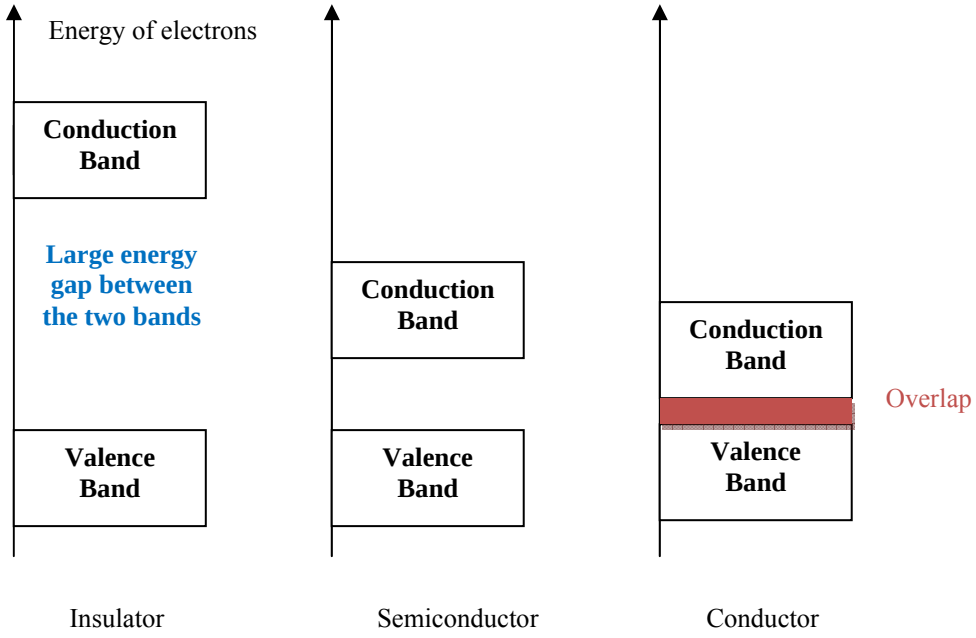

Figure 1. Energy bands in solids

A photo excited electron in the valance band and its corresponding hole are bound to each other by an electrostatic attraction. This bound pair is called an exciton. The average physical separation distance between the electron and hole in the exciton is called the exciton Bohr radius. The exciton Bohr radius is different for all materials. In a

bulk semiconductor, the dimensions of the crystal are larger than the exciton Bohr radius. However, if the size of the crystal becomes smaller than the material's Bohr exciton radius, the electrons hole pairs in that material are said to be confined. This phenomenon of confinement of the electron hole pairs in different dimensions is called quantum confinement.

Quantum well

A quantum well is fabricated by sandwiching a narrow bandgap material between two wide bandgap materials.[10] This arrangement creates a potential well that confines electrons and holes to the narrow bandgap semiconductor material, forcing them to occupy a planar region. Thus a quasi-two dimensional structure is formed.

In order to determine the optical properties, the number of available states per unit volume per unit energy may be calculated and measured. The available states are first calculated in k-space and then the density of states (DOS) is calculated in terms of energy. The DOS is a function that shows the distribution of energy states in the system. The DOS for a quantum well is a step function with steps occurring at the energy of each quantized level. Figure 2 shows the dimensional confinement of a structure and the corresponding density of states.

Quantum wire

A quantum wire is a quasi one dimensional structure. In quantum wires, energy is quantized in two dimensions. The spatial confinement results in the compression of energy states within the bands. The confinement of material and the resulting density of states is shown in figure 2.

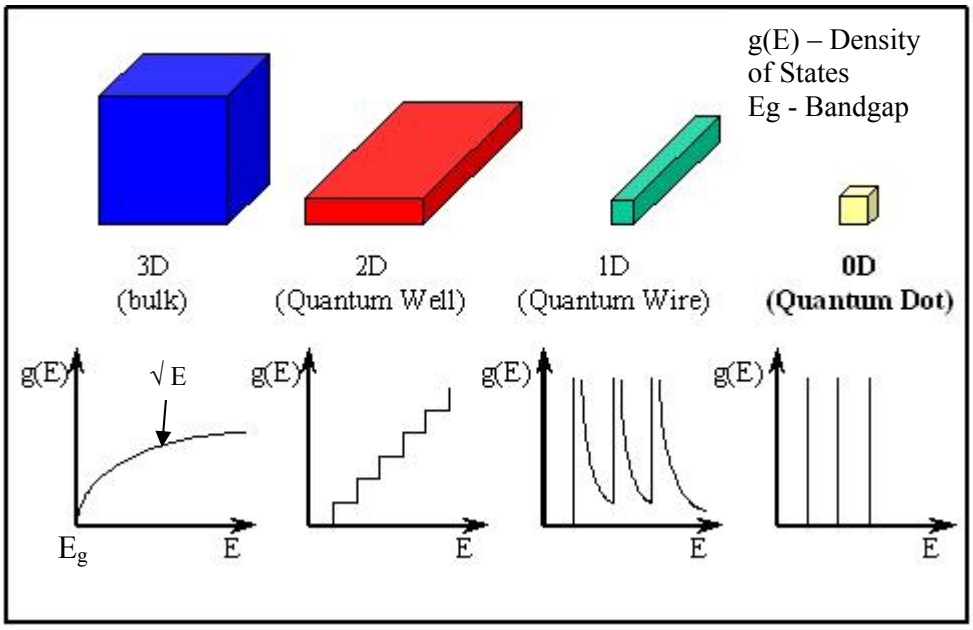

Structure	Degree of Confinement	Density Of States
Bulk Material	0D	$\sqrt{E}$
Quantum Well	1D	1
Quantum Wire	2D	$1/\sqrt{E}$
Quantum Dot	3D	d(E)

Figure 2. Quantum confinement in different materials[13]

Quantum dots

A quantum dot is a semiconductor nanostructure in which the electron-hole pairs are confined in all three space dimensions.[11] The characteristic length or radius of a

quantum dot can be compared to the Bohr radius.[12] The quantum confinement results in narrow and discrete peaks in the density of states and causes a blue shift in the emission wavelength. A quantum dot is a quasi zero dimensional structures with sharp resonances conceptually similar to an atom as shown in figure 2. Ideally, the absorption lines would be delta functions for QD's. However, the actual transitions are both inhomogeneously and homogeneously broadened, and are therefore not delta functions.

The discrete energy states $E_{n,l}$ for an ideal spherical QD is given by[14],

$$E_{n,l} = Eg + \frac{1}{R^2}\left[\frac{1}{m_e} + \frac{1}{m_h}\right]\frac{h^2\alpha^2{}_{n,l}}{8\pi^2}, \quad (1)$$

Here E_g is the bulk energy gap, m_e is the electron mass, m_h is mass of the hole, R is the radius and $\alpha^2{}_{n,l}$ is the n^{th} root of l^{th} order Bessel function.

The quantum confinement effect allows effective tuning of the emission and absorption wavelengths of QD's as a function of their size. The larger the QD, the smaller it's transition energy resulting in longer emission wavelengths. As the size decreases, the confinement increases and therefore the emission is blue shifted.

Fabrication of QD's

There are numerous methods to fabricate quantum dots. The three most commonly used synthesis methods are:

1) Epitaxial QD synthesis
2) Aqueous synthesis
3) Organometallic QD synthesis

- *Epitaxial QD synthesis*

QD's are prepared using the Stranski-Krastanow growth mode using strained InGaAs on GaAs and SiGe on Si.[10, 15] Self assembled QD's nucleate under certain growth conditions using molecular beam epitaxy (MBE). When a semiconductors lattice structure does not match that of a material and when the semiconductor material is grown on that substrate, the strain that results due to the lattice mismatch produces QD's.[16] However, the QD's fabricated using this technique are not used in biological research as it is not biocompatible. The QD's fabricated using MBE are also very expensive due to the cost of the MBE system. The quantum dots prepared using this method are defect-free and can be incorporated coherently into the host material, which makes them potential candidates for electronic and optoelectronic applications.

- *Aqueous synthesis of colloidal QD's*

Synthesis of colloidal QD's by aqueous chemistry involves the use of low temperature polar solvents like methanol or water. For example, reverse micelles (nano-reactors) can be used for aqueous growth of QD's.[17] As micelles bump into each other, they exchange material and QD's begin to grow. The temperature of the synthesis is limited by the boiling point of the solvent that is used for the synthesis.[18]

- *Organometallic QD synthesis*

Quantum dots can be fabricated colloidally using both hot and cold organometallic synthesis. There are three steps involved in the preparation of QD's:

Nucleation

Growth

Quenching the growth

The QD's prepared by the hot organometallic method utilizes non polar solvents such as trioctylphosphine oxide (TOPO)[19-21], dodecylamine or stearic acid.[22] High temperature growth anneals the QD's producing a more crystalline material. As produced, the QD's fabricated using the organometallic technique are not water soluble and therefore not biocompatible. The space required for this fabrication method is considerably smaller than that required for MBE. Additionally, these QD's initially have a relatively low quantum yield.

- *Colloidal core/shell QD's*

This work involves the preparation of Cadmium Selenide (CdSe) QD's with an organic coating of TOPO and an additional Zinc Sulfide (ZnS) capping layer. The ZnS capping layer passivates the surface of the QD core, and increases the quantum yield and luminescence.[23] Quantum yield is defined as the ratio of the number of photons emitted to the number of photons absorbed. The ZnS coating also reduces blinking which can be one of the disadvantages in using QD's.[24] Again, the ZnS coated QD's are not water soluble as produced. A number of methods can make the QD's water soluble. One of the methods to make them water soluble is the ligand exchange method in which a layer of mercaptoacetic acid (MAA) or dihydrolipoic acid (DHLA) is coated over the QD's.[25]

Advantages of QD's over traditional organic fluorophores

QD's have several advantages over organic fluorophores and they have the potential to replace organic dyes in many biological applications. The advantages include:

a) Narrow emission spectrum

b) Broad absorption spectrum

c) Photobleaching resistance

d) Size-tunable absorption and emission spectra

e) High quantum yield

a) Narrow emission spectrum

The emission spectrum of a sample QD is very narrow and symmetric compared to organic fluorophores if the sample has monodisperse size distribution, as little as 5% variation in diameter. Due to the band structure, electrons (holes) scatter to the bottom (top) of the conduction (valence) band before recombining. Therefore the QD's will always emit from the lowest energy state. This results in a spectral width under 40 nm FWHM; making the QD's ideal for spectral multiplexing. Spectral multiplexing, involves the simultaneous observation and spectral separation of a number of distinct QD populations. Figure 3 shows the linear absorption and emission from a sample of QD's. This emission has a FWHM of approximately 40 nm and is symmetric about the center wavelength of QD emission spectrum.

b) Broad absorption spectrum

QD's possess very broad excitation spectra and can be excited with simple excitation sources at essentially any wavelength shorter than the emission peak.[26] This facilitates simultaneous excitation detection, imaging and quantification of QD populations.

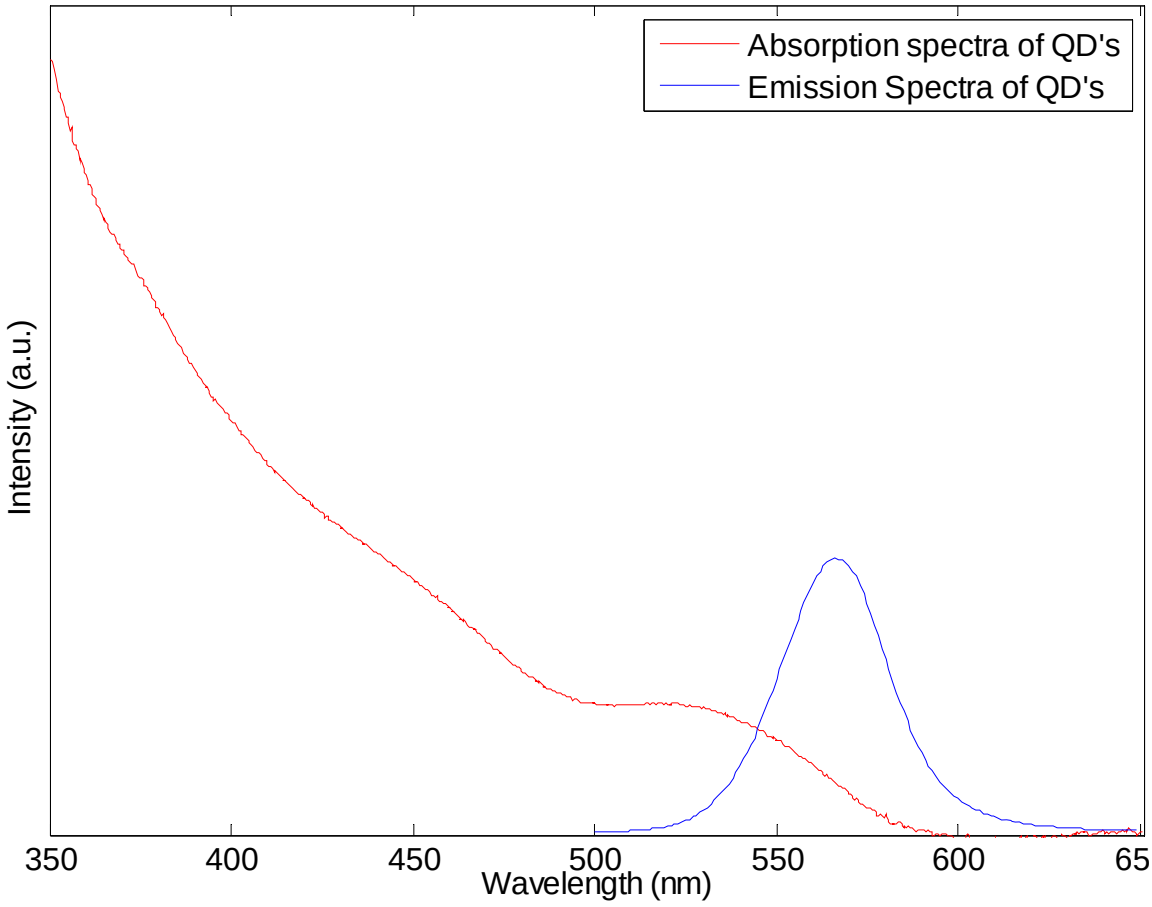

Figure 3. Comparison of absorption and emission spectrum of QD's

In the case of traditional dyes, the emission and absorption peaks are close to each other. Stokes shift is the wavelength or frequency difference between positions of the absorption peak and emission peak. If the first absorption peak in the QD sample is considered, the Stoke's shift in QD's is much smaller than that of organic dyes. However, the broad absorption spectrum allows us to choose an excitation wavelength that produces a large effective Stoke's shift. The very low spectral overlap of the emission spectrum of different colored QD's is a very useful property for spectral

multiplexing. A sufficient Stokes's shift is essential for spectral multiplexing applications.

c) Size-tunable absorption and emission spectra

From equation 1, the QD's lowest energy state (from which it emits) is inversely dependent on size. Thus it is possible to control the output wavelength of QD's by changing the QD size. Emission spectra from different size QD's is shown in figure 4. The size of QD's can be controlled by the temperature of the reaction, by the type of organic solvent used, and by the duration for which the reaction is run. Thus, through size tunability, QD samples can be fabricated to emit narrow color spectra that are spectrally distinct and may be excited by a single excitation wavelength.[22] This property of size tunability also makes QD's a good donor in Förster Resonance Energy Transfer (FRET) applications.

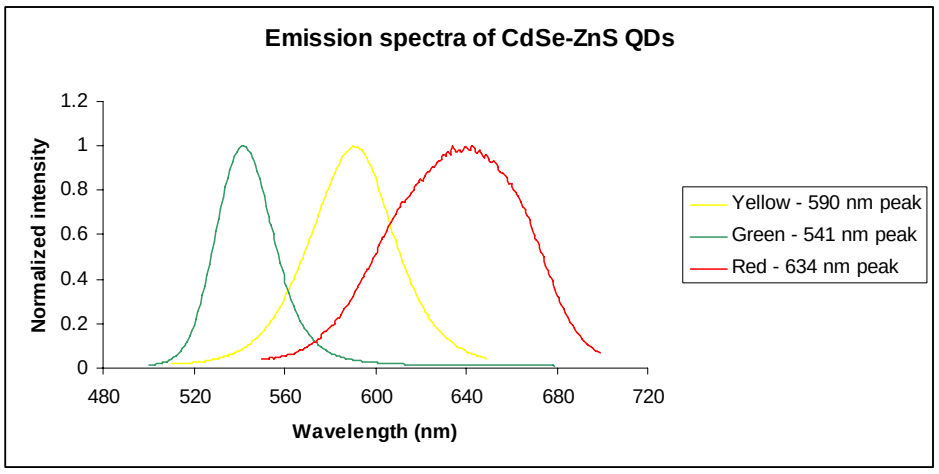

Figure 4. Size tunable emission spectra of QD's[8]

d) Photobleaching resistance

One of the main advantages of QD's is high photostability when compared to organic fluorophores. Wu *et al*[7] studied the comparison of photostability between an organic dye (Alexa 488) and CdSe/ZnS QD's. In their work, they labeled nuclear antigens with QD-streptavidin emitting at 630 nm and microtubules with Alexa 488, conjugated with IgG, having an emission peak at 488 nm. The specimens were illuminated for 3 minutes with a 100 W mercury lamp. They observed that the signal from Alexa 488 faded completely within 2 minutes while the QD's show little, if any, photobleaching. They repeated the same procedure with a reversal of the labels on nuclear antigens and microtubules. Again, Alexa 488 underwent significant photobleaching within the first 2 minutes of illumination while the QD's were extremely stable throughout the observation time. When a molecule has to be tracked for an extended period of time, photostability is a key factor to the success of the experiment. Thus, QD's provide superior performance as contrast agents compared with organic flurophores in long term biological applications such as medical imaging.

e) High quantum yield

Quantum yield is the ratio of the number of photons emitted to the number of photons absorbed. It has been found that the CdSe/ZnS QD's exhibit quantum yields of more than 80%.[27] This exceeds the quantum yield of traditional organic fluorophores such as TRITC and FITC.

Disadvantages of QD's over traditional organic fluorophores

There are a few issues that have restricted the use of QD's in biological applications. Oxidation of the CdSe or CdTe cores is known to release Cd^{2+} ions. Cd^{2+} ions are cytotoxic and none of the coatings have so far been reliable in containing ionic leakage. Various research groups[28, 29] have made efforts to coat QD's with different materials to make the QD's biocompatible. The release of cadmium and zinc ions is very toxic and therefore the use of QDs in long term *in vivo* applications has been restricted. Containing this ionic leakage is the center of much research and represents a major challenge to the use of QD's in biomedical applications.

Principle of photo-luminescence

Photo-Luminescence is the process in which a molecule excited by electromagnetic radiation releases energy in the form of light.

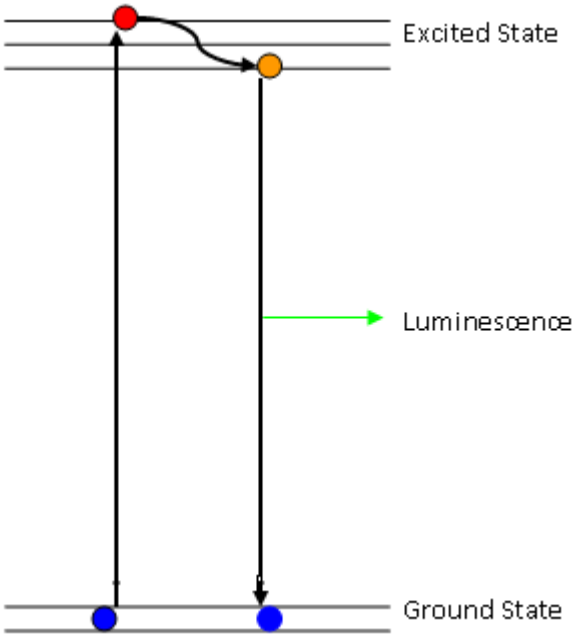

Figure 5. Simplified energy diagram

In general, a molecule is raised to an excited state via absorption of a high energy photon. The process is illustrated using a simplified energy diagram shown in figure 5. In this diagram, an incident photon is absorbed by the QD and raised to an excited energy state. Excited carriers at energy well above the band edge scatter or relax to the bottom of the band. Vibrational relaxation plays a major part in this process. In QD's this is accomplished via lattice vibrations or phonons. The emission, which is termed luminescence, has a width that is primarily dependent on the size distribution of the ensemble of emitting QD's and wavelength determined by the bandgap/size of the QD's.

Nonlinear optics

In classical non-linear optics, the polarization **P** of any medium is expanded in powers of the electric field vector **E**:

$$\mathbf{P} = \chi^{(1)}\mathbf{.E} + \chi^{(2)}\mathbf{.EE} + \chi^{(3)}\mathbf{.EEE} + \cdots$$

where $\chi^{(n)}$ is the n-th order nonlinear susceptibility.[12, 30] Linear optics are governed by the first term. For a linear response, the polarization of the molecule is linearly proportional to the applied electric filed. There are two main nonlinear optical processes used in microscopy.

1) Second harmonic generation (SHG)
2) Multiphoton Microscopy

Second harmonic generation

SHG is a case of sum frequency mixing where the frequencies of the photons from the two incident beams are equal ($\gamma_1=\gamma_2$). Crystal materials lacking inversion symmetry can exhibit $\chi^{(2)}$ nonlinearity. An input (pump) beam generates another beam

with twice the optical frequency in the medium. In SHG, several photons interact with a molecule simultaneously with no absorption events thus avoiding complications of photochemistry. SHG is efficiently used for detecting changes in membrane potential as it is very sensitive to biological membranes. It is also used in selective corneal imaging and many other applications. The process of SHG is illustrated in figure 6.

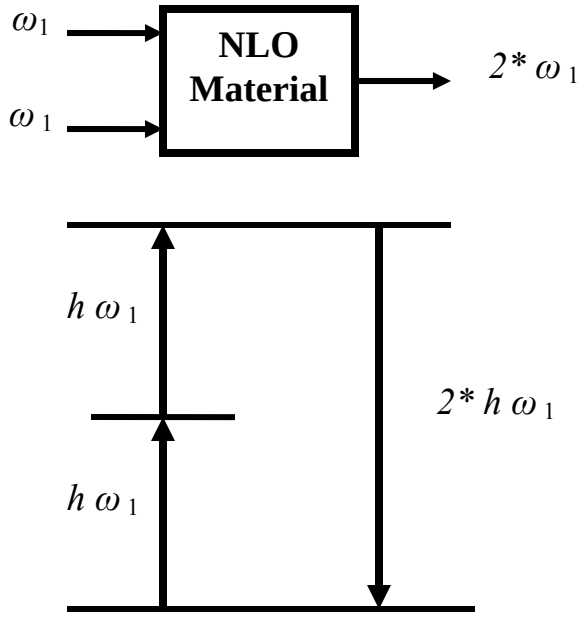

Figure 6. Second harmonic generation[31]

Multiphoton microscopy

In her 1931 doctoral dissertation, Maria Goppert-Mayer predicted that an atom or a molecule could absorb two photons simultaneously in the same quantum event.[32] However, her hypothesis was not confirmed until the invention of ruby lasers in the early 1960's.[33] The two photon excitation (TPE) cross section of different materials has been

determined using a number of different methods.[34-36] Denk et al. applied TPE luminescence to laser scanning microscopy.[37] TPE is a third order nonlinear optical process, which is described by the third order nonlinear optical susceptibility $\chi^{(3)}$.

When the photon density is very high, two photons can be absorbed simultaneously to a real excited state. The electronic transition of a lumiphore to the higher energy state takes place as a result of the combined energy of two photons. As the wavelength and energy of a photon are inversely proportional, both the photons should have about twice the wavelength of the photon that is required for a single photon excitation. The absorption of the two photons is mediated by a virtual state. As an example, two near infrared photons are required to combine to excite a blue absorbing fluorophore.

The simplified energy diagram shown in figure 7 consists of an initial state $|I\rangle$, a final state $|F\rangle$, and a manifold of virtual states $|V\rangle$ represented by dashed lines. Virtual states are determined by the spectral characteristics of the pulse and by the material. Two photon absorption (TPA) is facilitated by both degenerate and non degenerate frequency mixing. If the two photons that are absorbed are of the same wavelengths, the process is termed as degenerate TPA. This essentially means that for degenerate TPA, the virtual state lies halfway between the initial and final states. If the two photons absorbed possess different wavelengths, the process is defined as non degenerate TPA. Because of its broad spectral width, there is a possibility of more non degenerate transitions in broadband excitation than in narrowband excitation. Therefore, the probability of two photon absorption is greater when using a broadband femtosecond pulse.

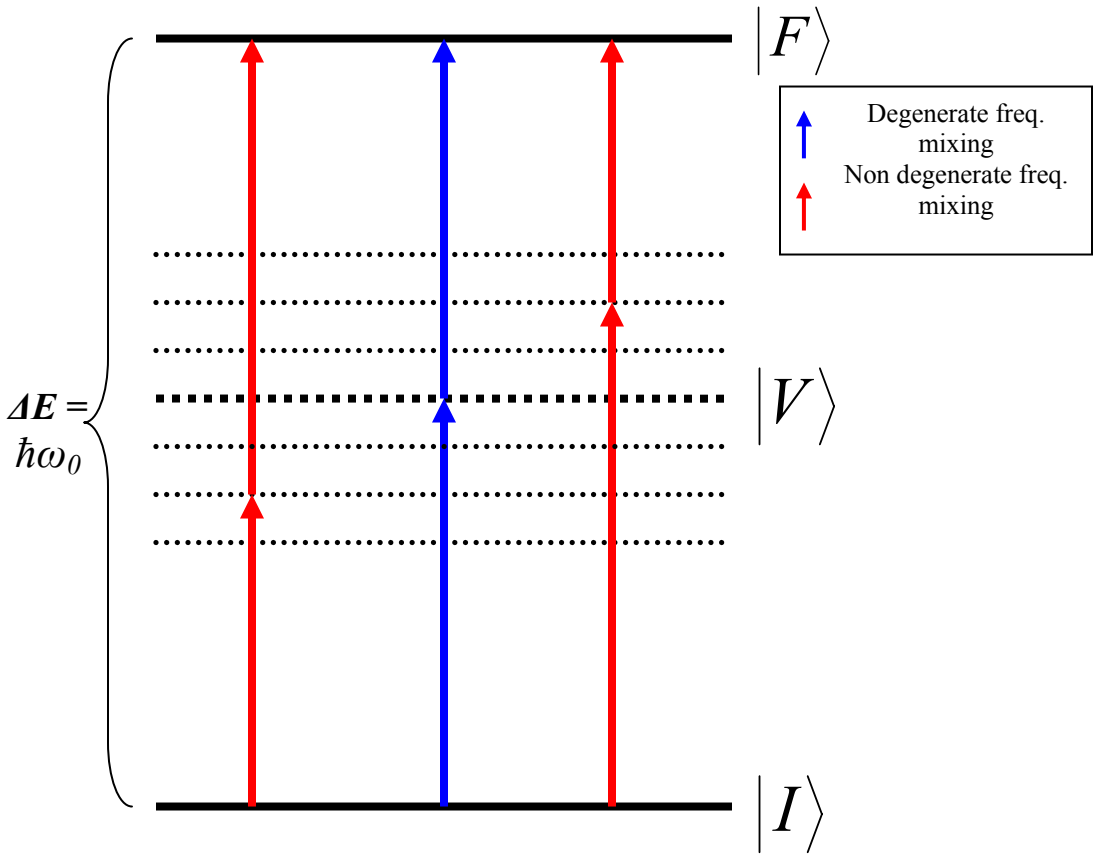

Figure 7. Degenerate and non degenerate TPA

The probability of TPA can be represented as

$$\Gamma \propto \left| \sum_V \left\{ \frac{\langle F|\mu \bullet E_a|V\rangle\langle V|\mu \bullet E_b|I\rangle}{\varepsilon_V - \varepsilon_I - \hbar\omega_b} + \frac{\langle F|\mu \bullet E_b|V\rangle\langle V|\mu \bullet E_a|I\rangle}{\varepsilon_V - \varepsilon_I - \hbar\omega_a} \right\} \right|^2, \quad (2)$$

$\mu \bullet E_{a,b}$ is the scalar product of transition dipole moment and electric field

for degenerate two photon transitions, $\omega_a = \omega_b$ and for non degenerate TPA, $\omega_a \neq \omega_b$

Degenerate TPA can be represented by just using the first term in equation 2.

This representation is fair for systems that use a narrow bandwidth as the probability of non degenerate excitation is very small in these cases. When calculating the probability of two photon absorption using an ultrashort pulse, both terms in equation 2 have to be considered in order to include non degenerate excitation.

Previously, enhancement in luminescent intensity was accomplished by chirping short pulses.[3, 38] The temporal shift of the frequency components in chirped pulses reduces non degenerate contributions.[39] In this work we compare, the enhancement in two photon excited luminescence from QD's while using near transform limited experimental 10 fs and 170 fs pulses. Transform limited pulses have the minimum pulse duration that is possible for a given pulse spectrum. Non transform limited pulses can generally be brought to their transform limit by modifying the phase of the spectral components. When using a transform limited pulse, the non degenerate components are maximized.[40] Therefore, luminescence intensity is increased when using a transform limited pulse.[38, 41, 42]

When the absorption cross section is uniform over the pulse spectrum, it can be shown that the transition probability (and therefore the luminescence) will increase as τ_p^{-1}, [3, 40] where τ_p is the pulse duration. Recently, extensive work has not been done to explore the effect of transform limited short pulse on TPE luminescence as it is difficult to maintain a near transform limited pulse at the focus due to the dispersion from the optical system.[43-45] Deviation from the τ_p^{-1} is expected for ultrashort pulses when the spectral width of the pulse exceeds that of the two photon absorption profile.[40]

Advantages of two photon microscopy

For optical sectioning, the two photon laser scanning microscopy technique has many advantages over the conventional confocal luminescence microscopy. The primary advantage lies in the ability to provide better optical sectioning at greater depths in thick specimens.[37, 46, 47]

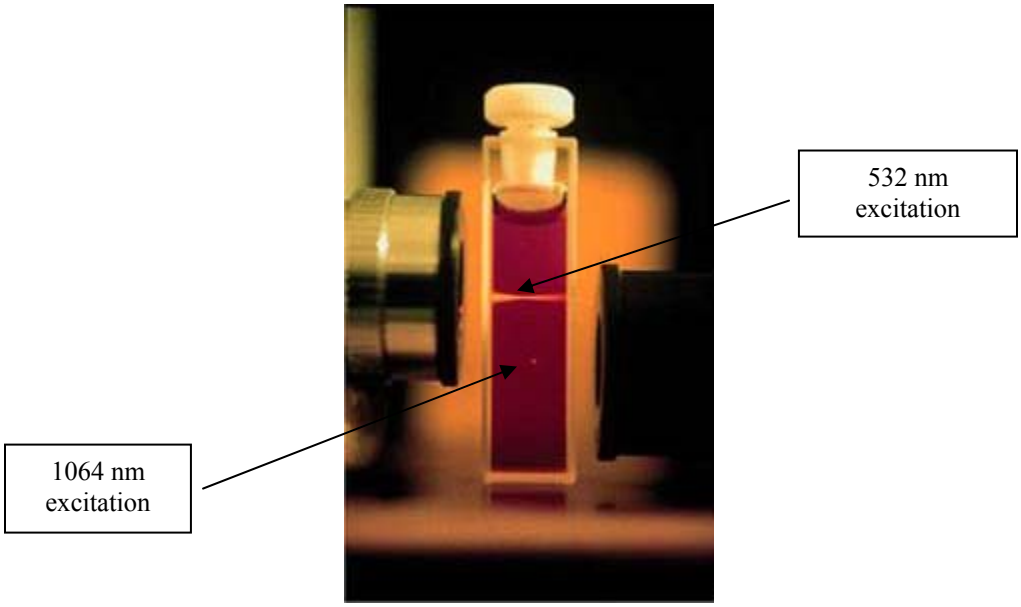

Figure 8. Picture illustrating two-photon and single-photon luminescence induced by a focused laser beam[48]

The most important difference compared to single photon absorption is the quadratic dependence of luminescence on the average power. Another major advantage is the localization of excitation in the two photon technique.[46] In two photon absorption, the number of absorbed photons, N_{abph} is described by the following equation:

$$N_{abph} = (\sigma P_{avg}^2 \pi^2 NA^4) / (\tau_p f_p^2 h^2 c^2 \lambda^2),^{48}$$

Where σ is the two-photon absorption cross-section, P_{avg} is the average power, NA is the numerical aperture of the objective, τ_p is the pulse width, f_p is the repetition rate, c is the speed of light, and λ is the wavelength of excitation light. This equation assumes that the two photon excitation process is a resonant absorption process.

With confocal microscopy, a laser is focused to a volume in the sample and the sample fluoresces throughout the beam path because of the large probability of single photon absorption. In multiphoton excitation, as the probability of absorption decreases with distance away from the focal volume, only the focal volume is excited. Figure 8 shows the same dye excited by a 10264 nm laser pulse and a 532 nm laser pulse. It is very clear from the 1064 nm excitation that the probability of absorption decreases rapidly away from the focal volume and therefore we just see a small dot of excitation in the picture.

Resolution in two photon microscopy

In two photon microscopy, the axial and lateral resolution is a bit worse than that of confocal microscopy. This is due to the use of longer wavelength photons in two photon microscopy, and results in a larger point spread function. The emission signal to background ratio has to be high to differentiate the two signals. In the case of multiphoton microscopy the signal to background ratio is inherently large owing to a very little excitation of the fluorophores outside of the focal volume.

In a confocal microscope, both axial and lateral resolution is degraded by finite pinhole aperture, chromatic aberration and imperfect alignment of the optical system.[49] A confocal pinhole in a confocal microscope contributes to a high ratio. In the confocal

case, luminescence occurs and a pinhole is placed in front of the detector to eliminate out of focus luminescence. However, this pinhole not only eliminates the luminescence away from the focal point, but also scattered (diffused) luminescence from the focus. In a confocal microscope, only ballistic luminescence is only detected.[46] Due to the longer wavelengths in multiphoton microscopy, scattering in tissue is lower compared to the UV excitation in the confocal microscope. A comparison of confocal and multiphoton microscopes is shown in figure 9.

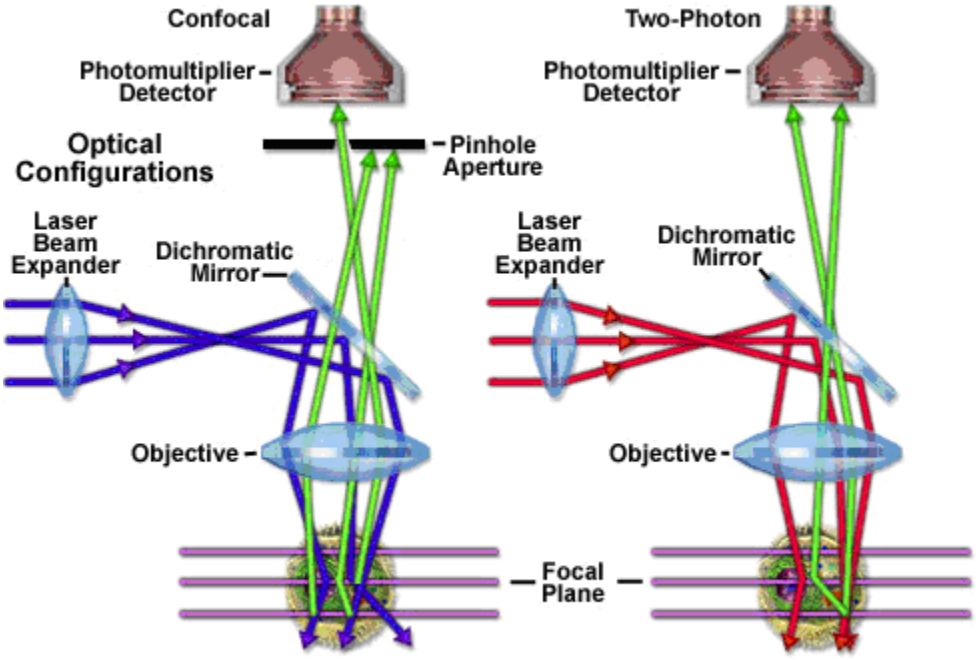

Figure 9. Comparison of excitation using confocal and multiphoton microscope[50]

Near infrared (NIR) radiation is used in multiphoton microscopy. Using NIR radiation to excite the sample has many advantages over the UV excitation. One of the

advantages is that the spectral range of 600-1100 nm is referred to as an optical window of cells and tissues due to the lack of endogenous absorbers in this spectral range and the resulting high penetration depth on the order of a few millimeters in most tissues.[51] Water has an absorption coefficient of about 0.1 cm^{-1} which is considered to be very low. Water is the major absorber in cells without hemoglobin or chlorophyll. These non pigmented cells are nearly transparent structures in the spectral range of 700-1100 nm.

EXPERIMENTAL DETAILS

Synthesis of quantum dots

Materials

Cadmium oxide powder, selenium powder, trioctylphosphine oxide (TOPO, 99% pure), cadmium oxide powder, selenium powder, and trioctylphosphine (TOP, 90% pure) were purchased from Sigma-Aldrich. Tetradecylphosphonic acid (TDPA, 98% pure) was purchased from Alfa Aesar. Methanol, ethanol, toluene, syringes and needles of different specifications were purchased from VWR. Hexamethyldisilathiane and dimethylzinc (1 molar solution in heptane) required for the ZnS capping of CdSe quantum dots were also purchased from Sigma-Aldrich.

Set up

The experimental setup for the organometallic synthesis of CdSe/ZnS quantum dots is shown in Figure 10. A stir bar made from aluminum is connected to a drill press to stir the contents of the reaction sample. A heating mantle filled with molten bismuth alloy serves as the reactor. A temperature probe and controller are used to control the reaction temperature. To the side, a magnetic stir plate is used to stir the TOP-Se mixture. Argon, being heavier than oxygen, is used to drive out the oxygen from the reaction flask. An Argon bubbler was used to ensure a constant argon flow into the reaction glassware.

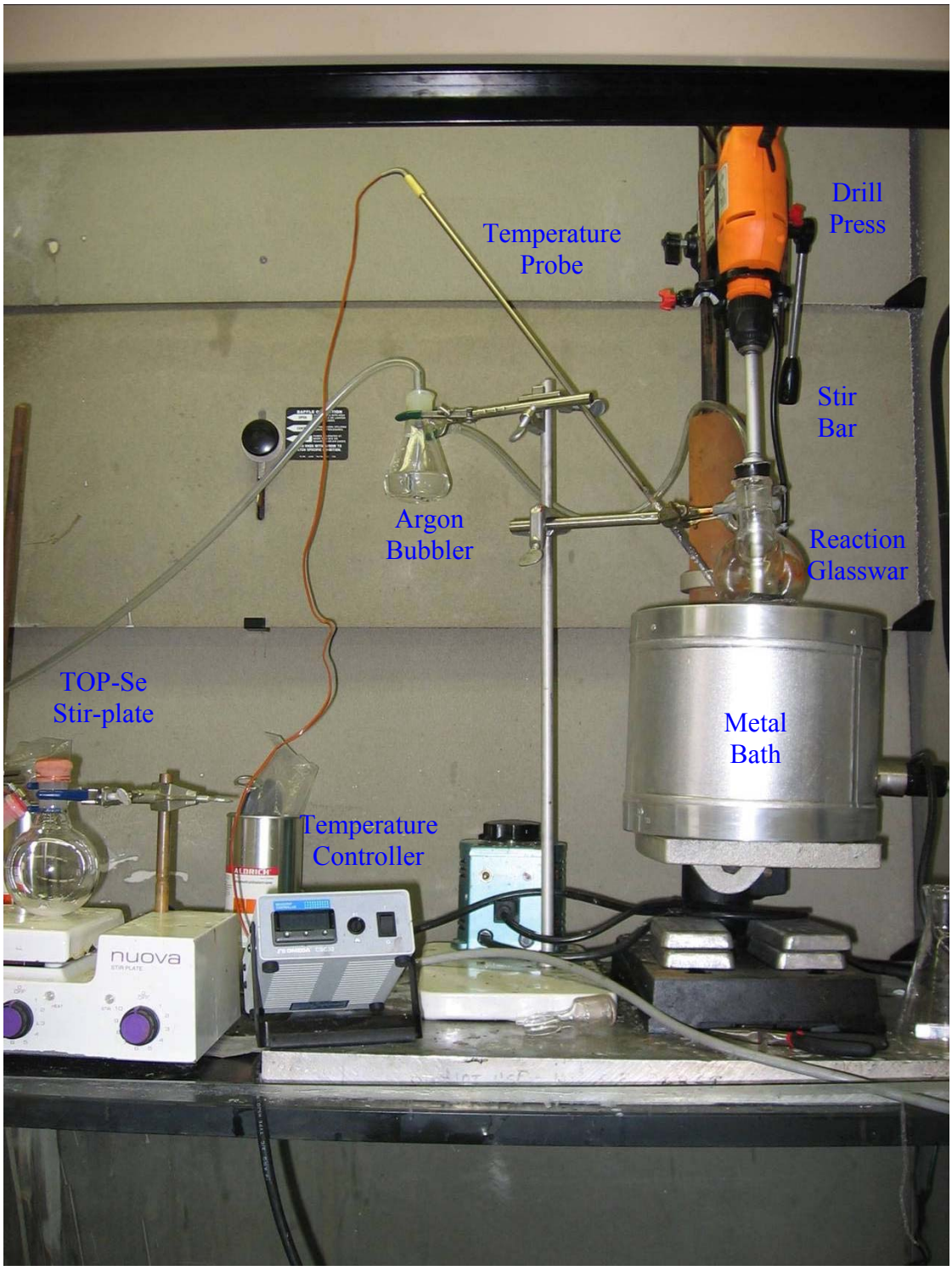

Figure 10. Reactor for the organometallic synthesis of QD's[8]

Methods

0.0514 g of Cadmium oxide (CdO), 3.7768 g of trioctylphosphine oxide (TOPO) and 0.0567 g of tetradecylphosphonic acid (TDPA) is heated under an argon blanket at 340°C until either the color changes from dark brown to nearly colorless or for a period of one hour. At this point, temperature of the Cd-TOPO solution is reduced to 270°C.[22] At the same time, 0.0411 g of selenium is stirred in 2.4 ml of trioctylphosphine (TOP) under argon until the selenium mixed with TOP.

At this point, the selenium solution is injected into the cadmium precursor and the reaction begins immediately. Samples are removed at various time intervals depending on the required size and color of the QD's. The QD's are then washed multiple times with methanol and toluene, and then suspended in toluene. Figure 11 shows emission from QD's fabricated from a single experiment and excited by a ultraviolet source.[52]

Figure 11. QD's suspended in toluene (taken from the Meissner lab)[52]

Capping of the CdSe QD's with ZnS structure is an additional procedure performed after fabricating the CdSe QD's. After the growth time required for QD's of a particular size is reached, the temperature is dropped to 200°C and a ZnS precursor solution, consisting of 1.6 ml hexamethyldisilathiane and 6.4 ml dimethyl zinc

maintained in an argon environment is injected. After allowing 1 hour for the shell to form, the temperature is reduced to 100°C to anneal the particles. Annealing is done for a period of 30 minutes, and then the CdSe/ZnS particles are quenched in methanol and cleaned according to the procedures described earlier for the CdSe/TOPO nanocrystals.

Two photon spectroscopy

Setup for the experiments

A schematic representation of the experimental set up is shown in figure 12. The narrowband laser used was a tunable Ti:Al_2O_3 oscillator (Mira 900F, Coherent) pumped by a frequency doubled Nd:YVO_4 laser (Verdi-10, Coherent). Center wavelength of 170 fs pulses was tuned between 700 and 890 nm in 10 nm increments which is approximately the bandwidth of the narrowband laser pulse. The pulse spectra of 170 fs laser from 790-800 nm and the spectrum of the 10 fs pulse are shown in figure 13. For the narrowband pulses, autocorrelation spectra were recorded for each wavelength step in order to ensure the pulses were approximately 170 fs. Since small amounts of dispersion introduced by the gain medium and other optical components in the laser system rapidly degrade the performance of the broadband pulse, dispersion compensating mirrors (-200 fs^2 per bounce) were used in the broadband configuration. These mirrors ensured a near transform limited pulse from the broadband Ti:Al_2O_3 oscillator (Femtosource, Femtolasers) at the focus. The broadband laser is not tunable as the spectrum contains almost the complete Ti:Al_2O_3 tuning range as shown in Figure 13.

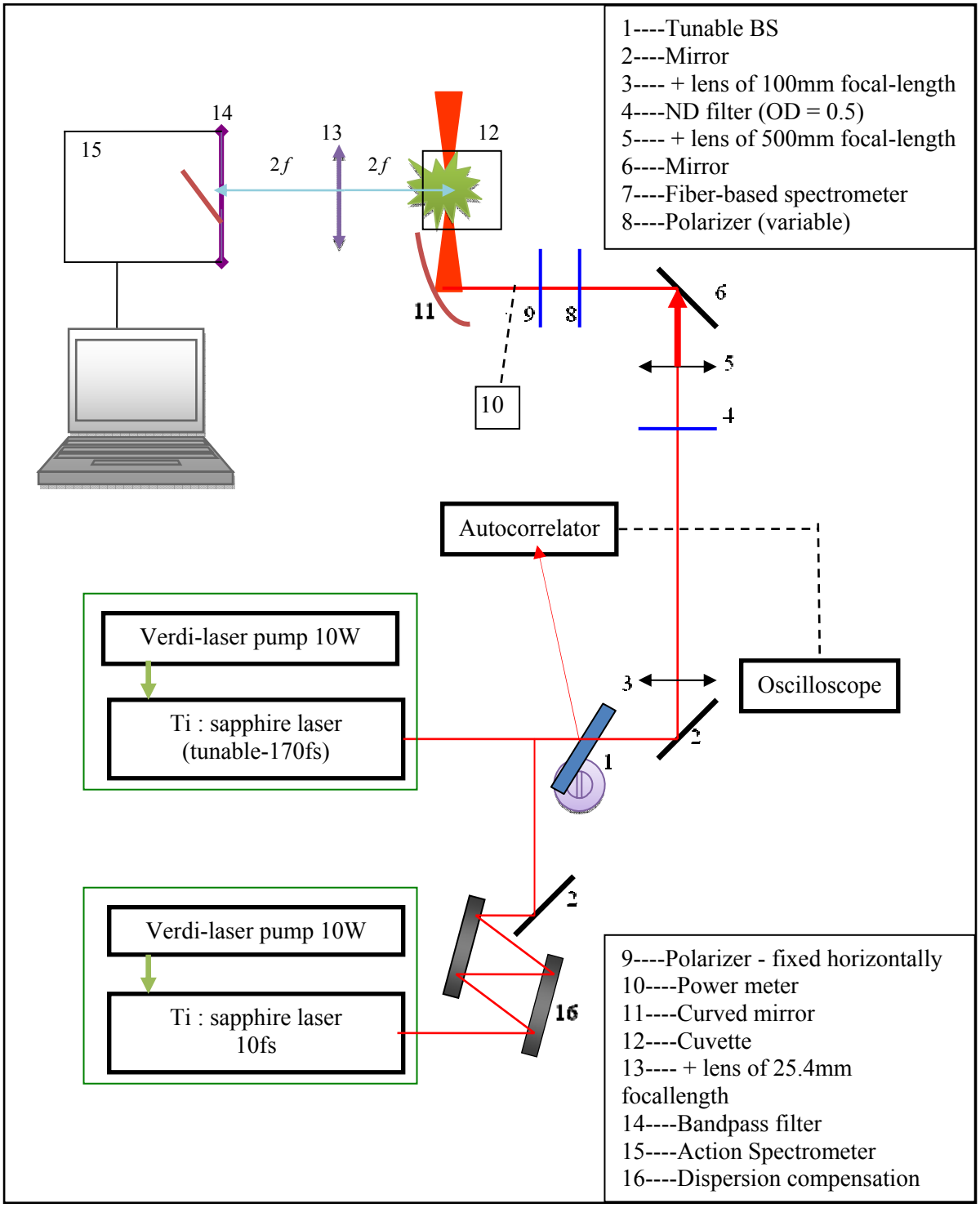

Figure 12. Experimental set up for measuring data with 10 fs and 170 fs oscillators

A curved mirror (focal length 25.4 mm) was used to focus the laser pulses into a 1 cm pathlength, fused silica cuvette. A beam expander was used to control the size of the laser beam so that the size of the beams from both the lasers closely matched. Two polarizers (Newport Inc) and one neutral density filter (Edmund optics) with an optical density of 0.5 were used to attenuate the laser power. Luminescence intensity from the QD's was collected using a thermoelectrically cooled detector array and spectrometer (Roper Scientific). Five average accumulations were taken with an integration time of 15 seconds for each accumulation. The slit width of the spectrometer was 300 microns. Slit width was set at 300 microns to make the spectral resolution approximately 3 nm (0.1*FWHM of QD's). The number of pixels required for this resolution was first calculated as

Number of pixels = 3nm/pixel-bandwidth = 3nm/0.208nm = 14 pixels

Each pixel is 20 microns. For 14 pixels, the slit width was 14*20 microns = 280 microns. Therefore, 300 microns was chosen. All the above calculations were based on the grating of 300grooves/mm at a 500nm blaze angle that was set for the experiments. The grating was shifted such that its center point was the emission peak of QD's.

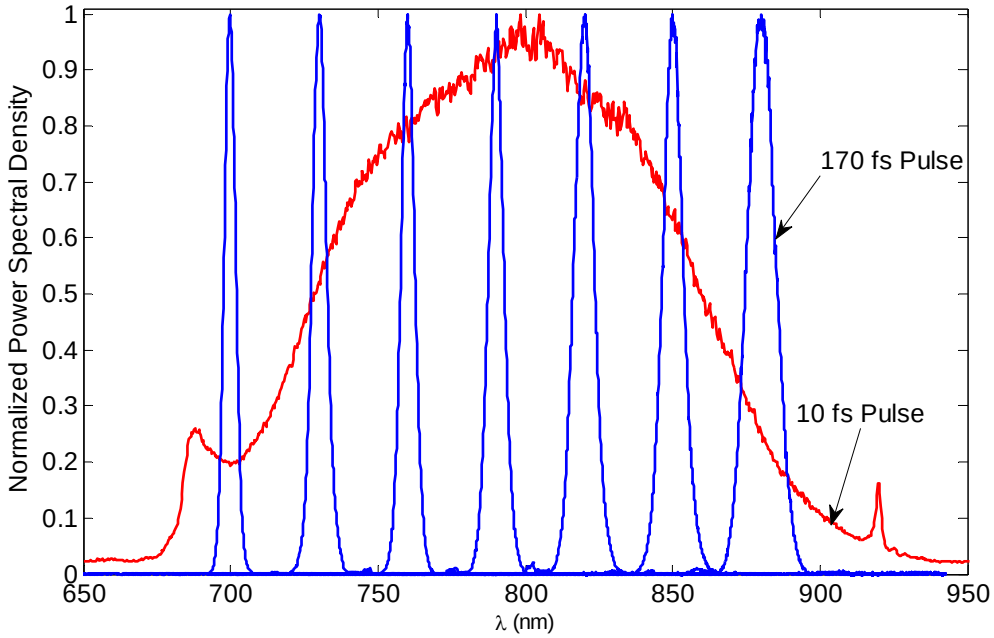

Figure 13. Spectrum of ~10 fs pulse and ~170 fs pulses

RESULTS

Experimental results

The first step is to verify the power squared dependence to confirm two photon absorption. For this, the average power of the broadband laser is varied from 10 mw to 100 mw and the luminescence from QD's is recorded for every 10 mw increment. When integrated luminescence intensity (I) is plotted against average laser power (p_{avg}) on a log scale, P_{avg} varies as $I^{2.06}$ for the 10 fs laser.

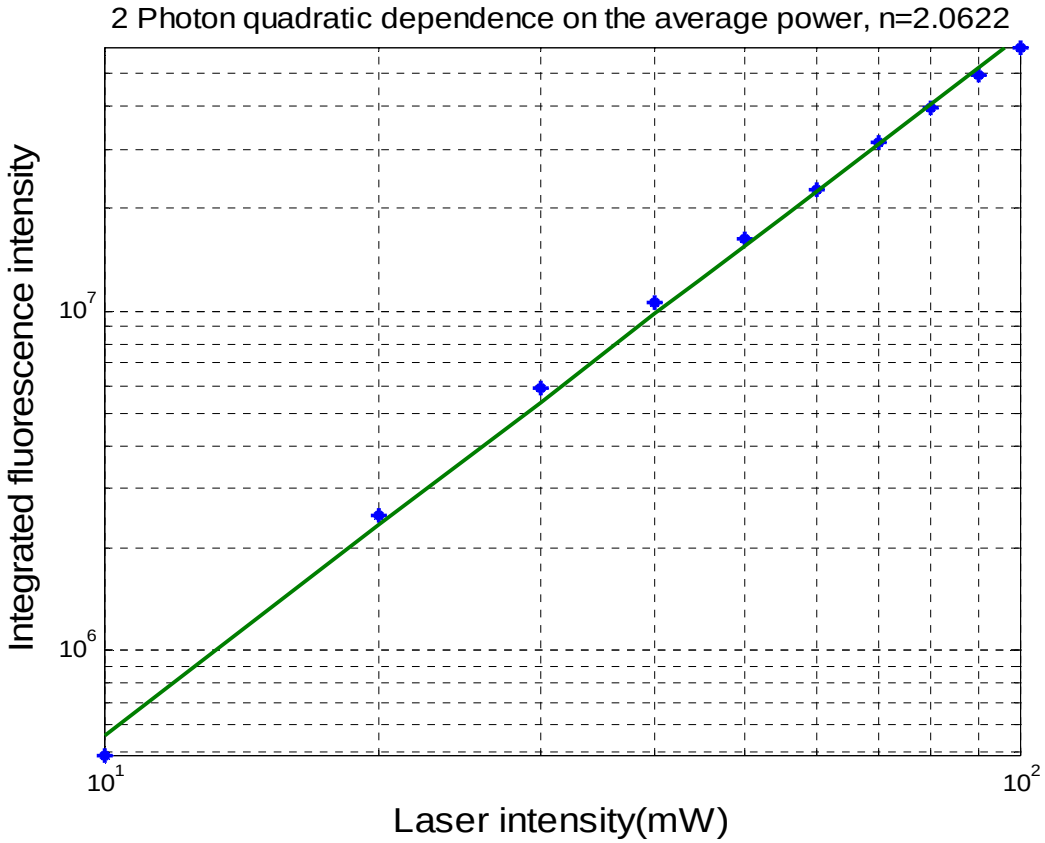

Figure 14. Verification of two photon quadratic dependence on the 10fs laser

To calculate the enhancement in luminescence from QD's, experimentally, the integrated luminescence emission intensity using both broadband and narrowband

excitations are recorded. The integrated luminescence intensity while using a broadband pulse as the excitation source is divided by the integrated luminescence intensity when using the narrowband source. The quotient is the enhancement in luminescence when using a broadband pulse compared to a narrowband pulse.

Figure 15. Verification of two photon quadratic dependence on the 170fs laser.

In the case of the narrowband laser, average power is varied from 150 mw to 350 mw and luminescence from the QD's is recorded for 10 mw increments. For the 170 fs laser, p_{avg} varies as $I^{1.77}$ with integrated fluorescence intensity. A log plot of the power squared dependence for the 10 fs laser and 170 fs laser are shown in figure 14 and 15 respectively. This verifies the I^2 relationship expected for two photon absorption.

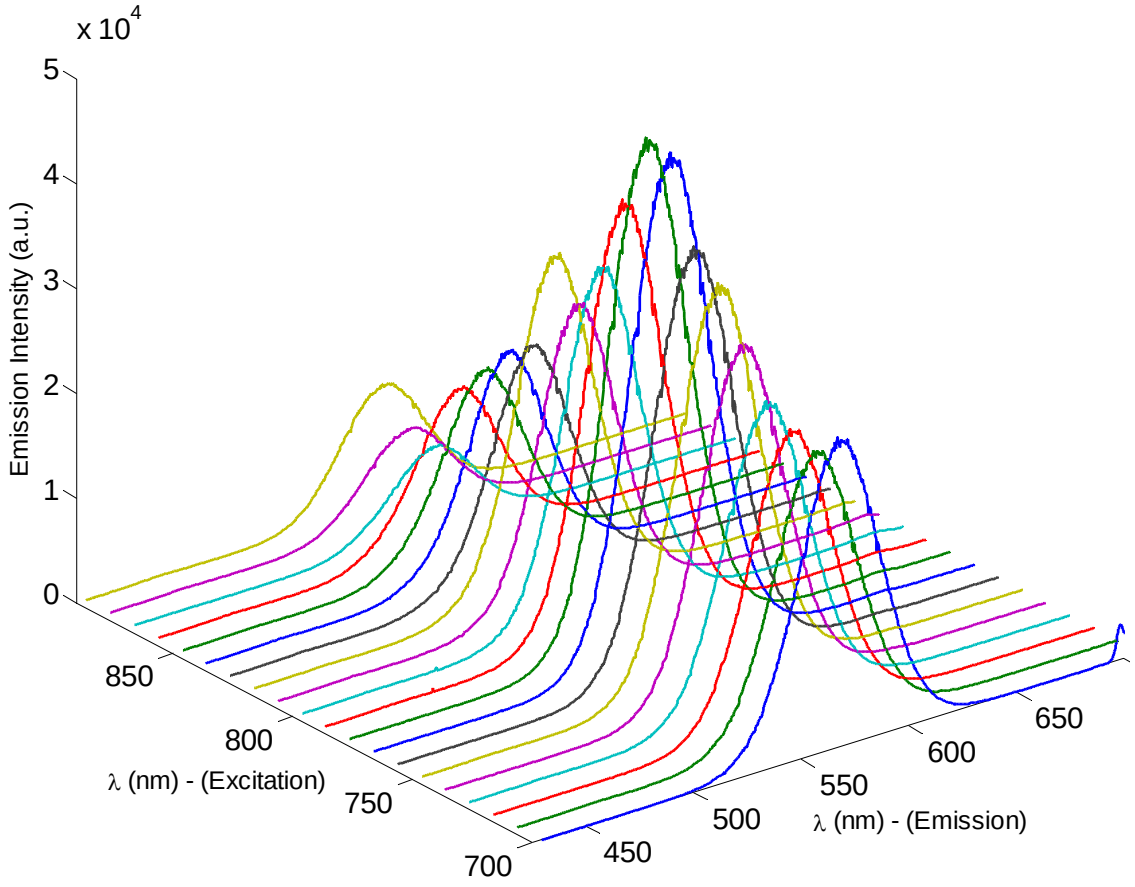

Figure 16. 3D plot of emission wavelength, excitation wavelength and Luminescence intensity

Luminescence intensity from the QD sample is measured from 170 fs pulses centered in increments of 10 nm from 700 to 890 nm. Figure 16 shows a 3D plot of the excitation wavelength, emission wavelength and luminescence intensity from the QD sample. From this figure we can see that the excitation peak for the QD's was 780 nm.

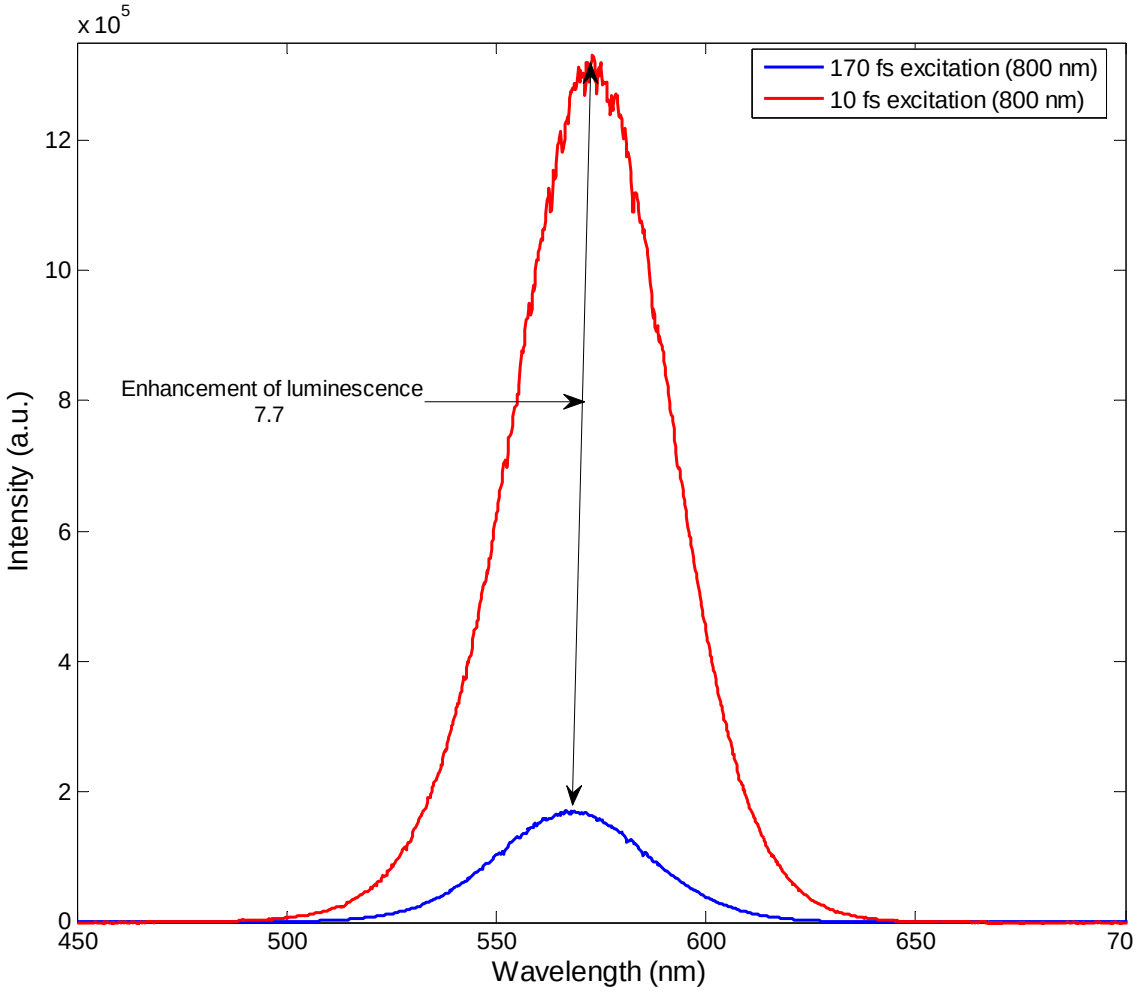

Figure 17. Enhancement in luminescence at 800 nm excitation

Experimental data is also measured on the QD sample using the broadband pulses (800 nm) in a similar way to the data acquisition using narrowband pulses. For the broadband laser, the pulse is centered at 800 nm as it is not a tunable laser. Using the data obtained from the experiments, the enhancement in luminescence intensity using the broadband pulse is calculated to be 7.7 more when comparing near transform limited 10 fs with 170 fs excitation as shown in figure 17. To find minimum enhancement, the QD emission peak excitation at the 780 nm peak for the 170 fs pulse is compared with the emission

from the 800 nm excitation of the 10 fs pulse. The enhancement in luminescence is 5.4 as shown in figure 18.

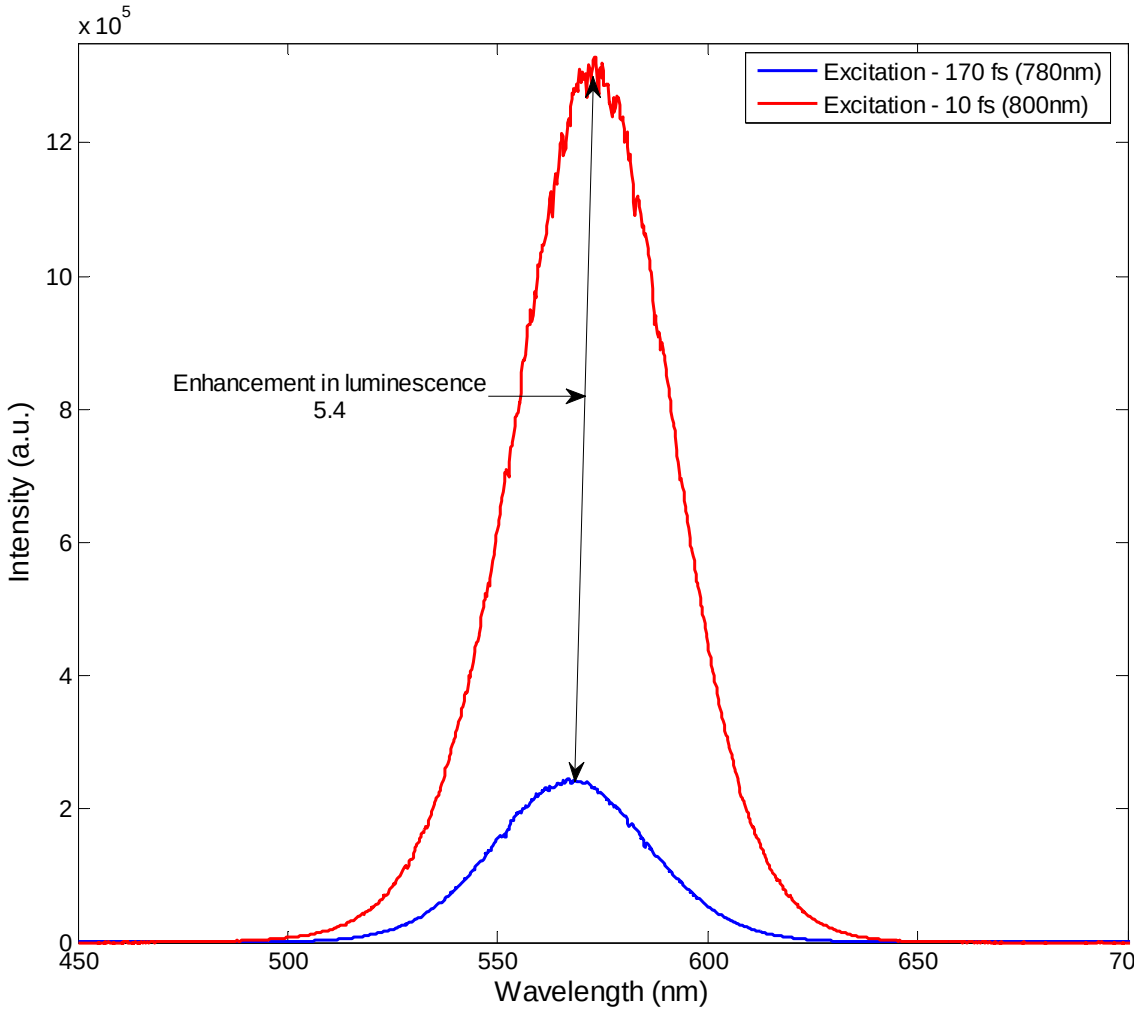

Figure 18. Enhancement in luminescence @ 780 nm (170 fs) and 800 nm (10fs) excitation

Theoretical results

Data from figure 16 is used to plot the two photon photoluminescence excitation spectrum (2PES). The normalized luminescence emission integrated intensity for each excitation wavelengths (700-890 nm) is taken and plotted against transition energy $((\Delta E/\hbar)*10^{15})$ to get the 2PES data points. For calculations, a sum of three Gaussian functions has been used to recreate the 2PES lineshape as shown in figure 19.

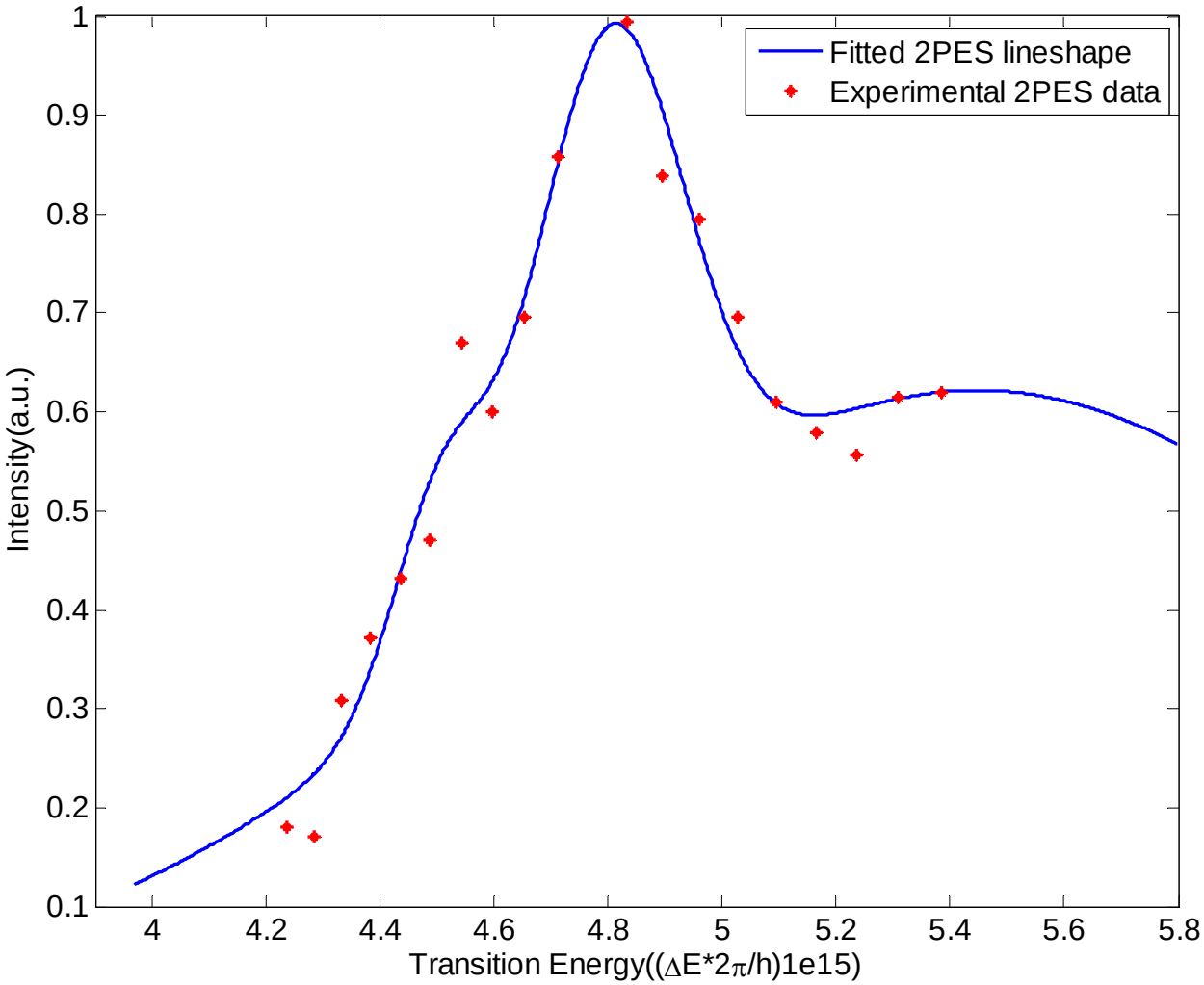

Figure 19. Two photon photoluminescence excitation spectrum

The entire two photon excitation spectrum for a pulse can be calculated as,

$$\mathrm{T}(\omega) = \left| \int_0^\infty E(\omega/2 + \Omega) E(\omega/2 - \Omega) d\Omega \right|^2, \qquad (3)$$

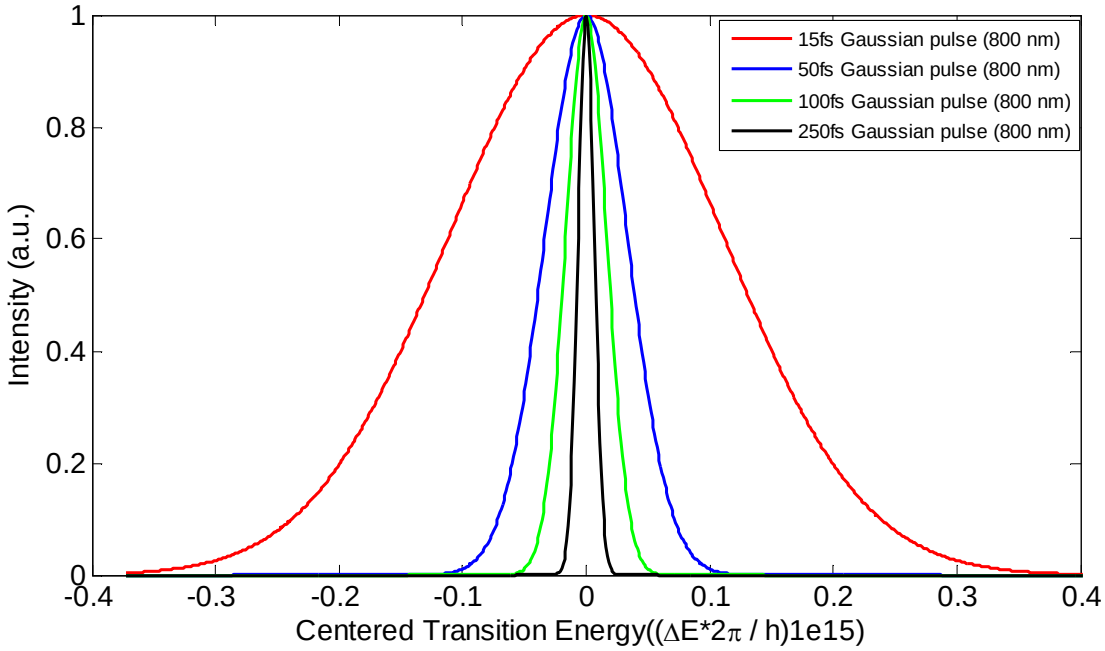

Figure 20. Two photon excitation spectrum (Gaussians)

Two photon excitation spectra (Gaussians) for different pulsewidths is shown in figure 20. The 2PES, $\gamma(\omega_0)$ as shown in figure 19 and the normalized pulse spectrum, from equation 4, were used for the calculation of transition probability of QD's as,[53]

$$\Gamma \propto \int_0^\infty \gamma(\omega_0) \left| \int_0^\infty E(\omega_0/2 + \Omega) E(\omega_0/2 - \Omega) d\Omega \right|^2 d\omega_0, \qquad (4)$$

where ω_0 is the transition energy. Equation 4 follows from second-order, time-dependent perturbation theory, assuming pulsed, non-resonant two-photon excitation.[53]

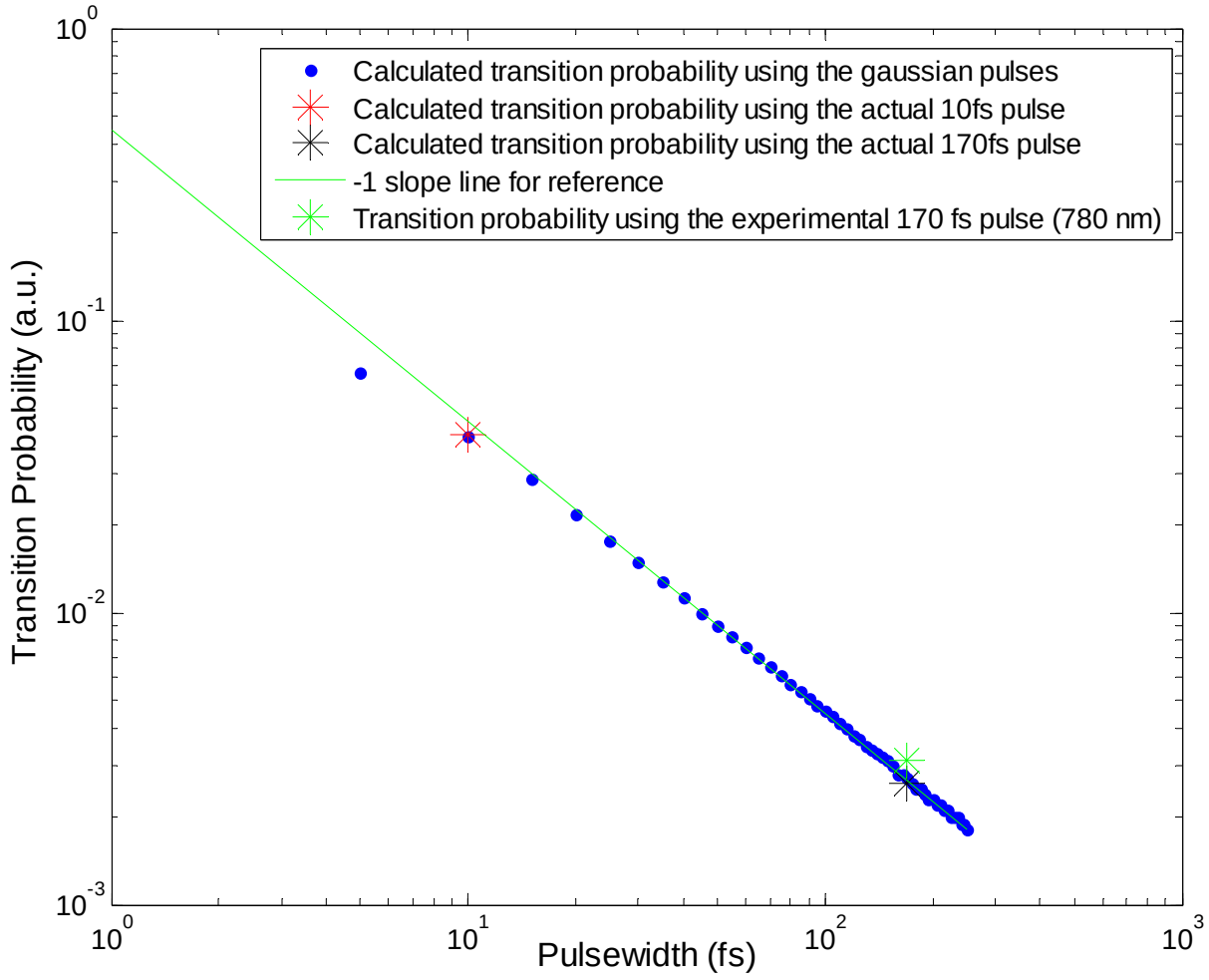

Figure 21. Two photon transition probability of QD's

A logarithmic plot of transition probability for QD's using Equation 4, the experimental pulse spectra (10 and 170 fs), and the 2PES is shown in Figure 21 (asterisks). A solid line with a slope of -1 is shown for reference. The blue dots in figure 21 are transition probabilities for different pulsewidths when using Gaussian pulses. The blue circle at 10 fs is the calculated transition probability using the experimental pulse (10 fs). The black

and red asterisks are the two photon transition probability calculated using 170 fs pulse centered at 780 nm and 800 nm respectively. The transition probability for QD's when excited by Gaussians centered at 800 nm, yields an enhancement of 14.92.

Transition probability when using the experimental pulses centered at 800 nm instead of the Gaussians yielded an enhancement of 15.65. The enhancement is 13.13 when comparing excitation from 170 fs experimental pulse centered at 780 nm and the 10 fs experimental pulse centered at 800 nm. For relatively narrow pulse spectra, the transition probability as a function of pulse duration follows a τ_p^{-1} relationship.[40] This relationship holds for pulse durations greater than 40 fs. Deviations begin to occur for ultrashort pulses.

Summary of results

Excitation Pulse	Experimental Calculations	Theoretical calculations using Gaussians	Theoretical Calculations using actual pulse
800 nm	**7.78**	**14.92**	**15.65**
780 nm (2PES peak)	**5.4**	**13**	**13.13**

Table 1. Summary of results

DISCUSSION

From the results, we see that there is an appreciable increase in the luminescence intensity of the QD's when using a 10fs pulse compared to a 170fs pulse. To verify if there was any shift or broadening of the emission spectra (figure 16), a plot of emission wavelength and power spectral density has been plotted for 3 excitation wavelengths (700, 800 and 890) for the 170 fs laser and 800 nm for the 10 fs laser as shown in figure 21. It is evident from the graph that there is no appreciable broadening or shifts observed.

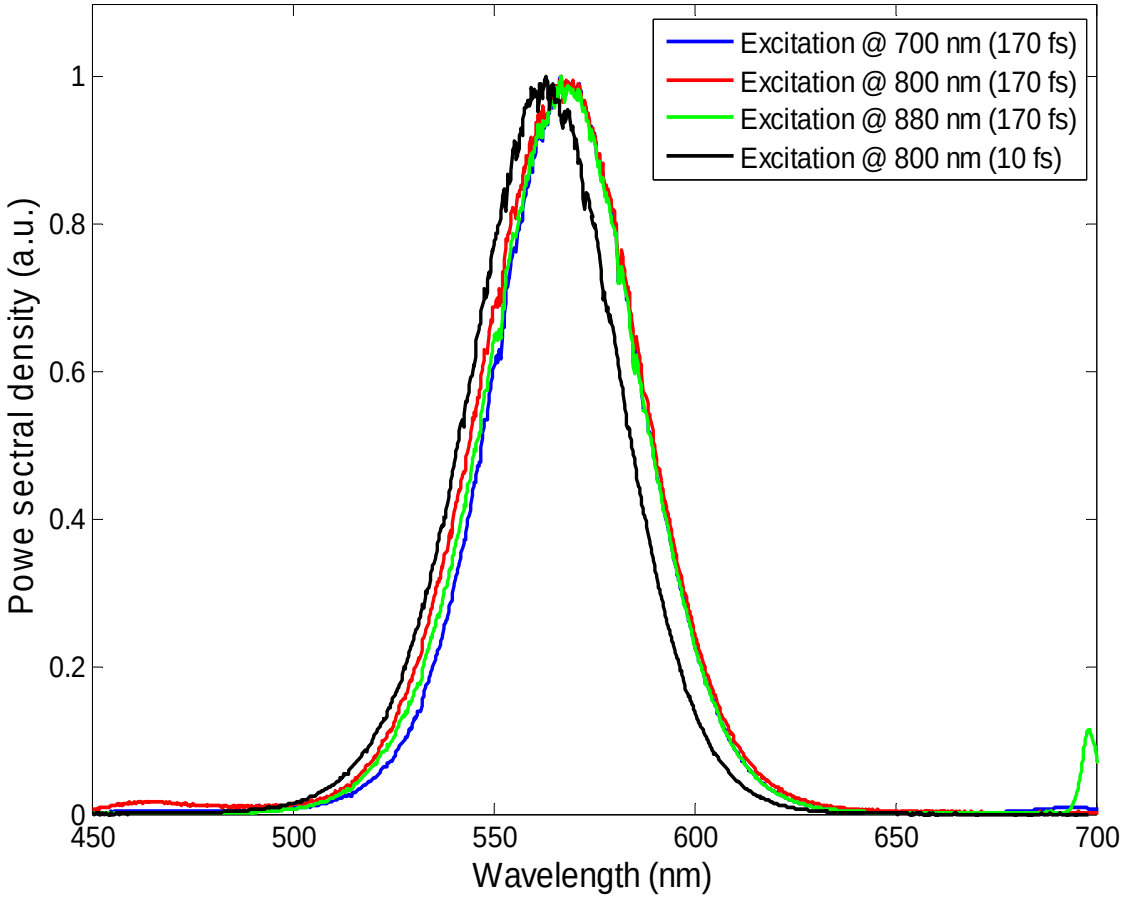

Figure 22. Normalized emission spectrum from QD's using 170 fs excitation @ 700, 800 and 890 nm

The 2PES spectrum (figure 19) was fitted so that the Gaussian peaks approximately corresponded to peaks/shoulders in the single photon absorption as shown by the arrows in figure 19.

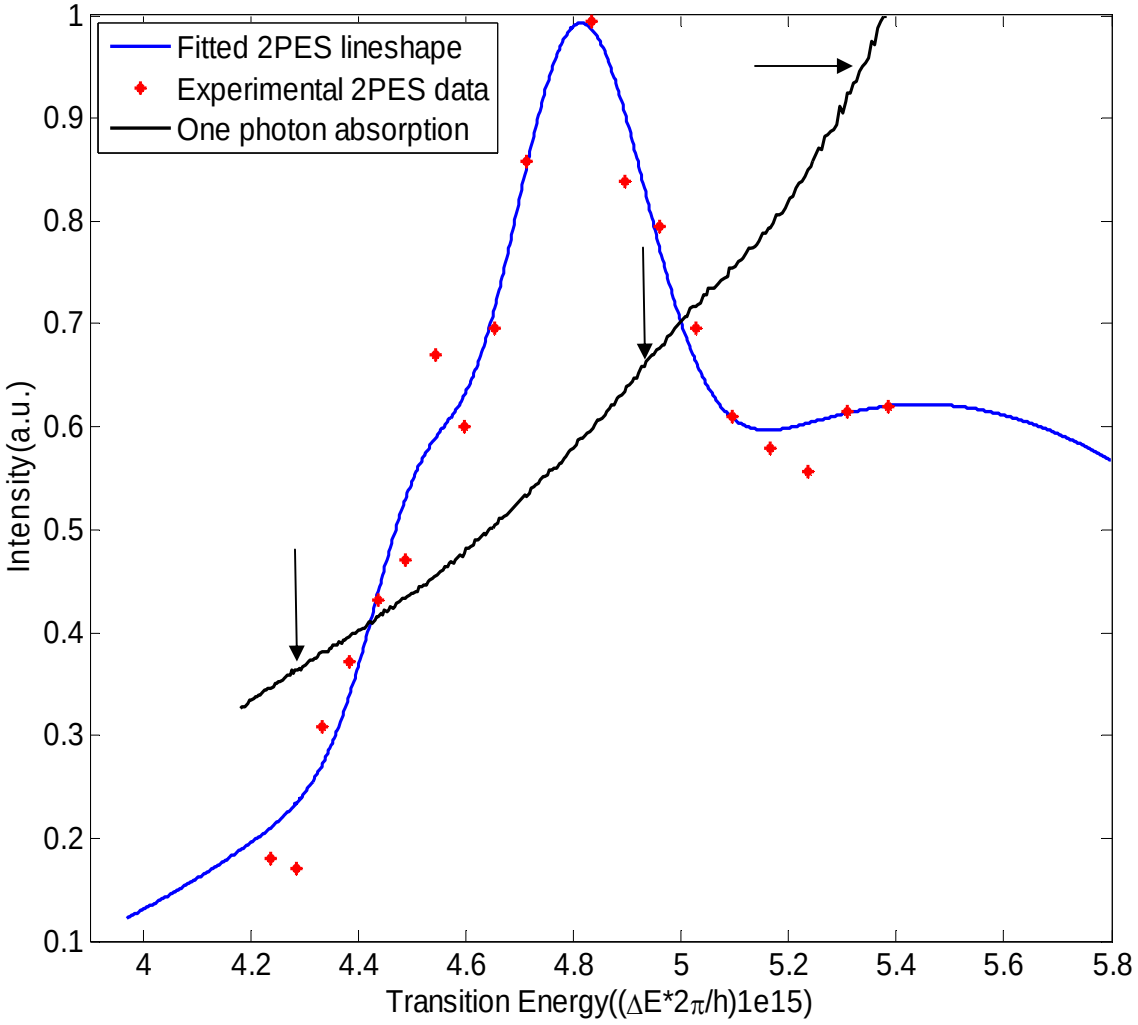

Figure 23. Comparison of single photon absorption and 2PES lineshape

The single photon absorption spectrum has three distinct peaks as shown with three arrows in figure 22. The 2PES spectrum for longer wavelengths (> 950 nm) were not predicted as our laser does not cover those wavelengths. Sums of 1-4 Gaussians were

investigated to determine the best fit for the 2PES spectrum. With an R^2 of 0.97, the sum of three Gaussians was the best fit.

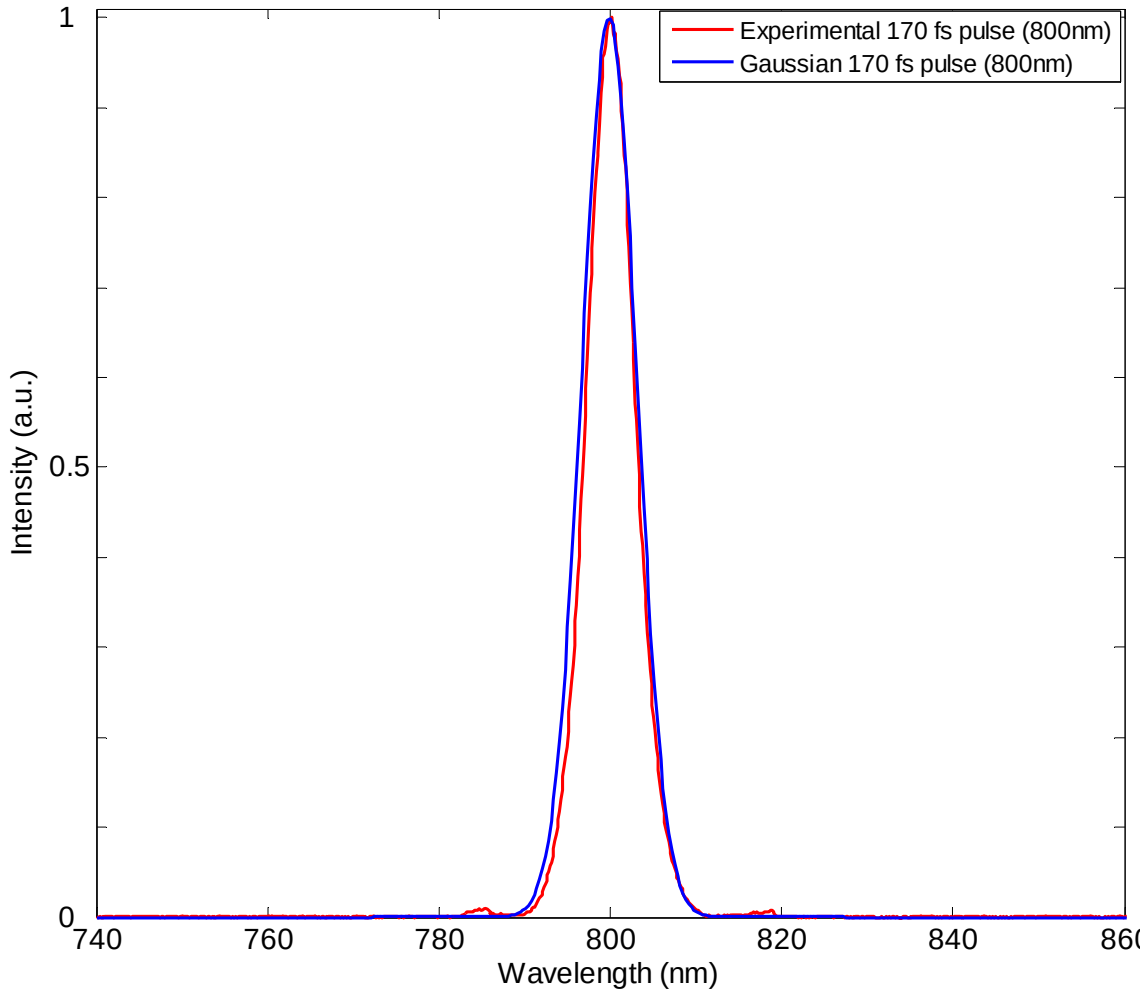

Figure 24: Comparison of Experimental and Gaussian 170 fs pulses

The transition probabilities for the experimental pulse spectra centered at 800 nm do not exactly match the values determined by the Gaussian pulses. It is interesting to note that the pulse spectrum of the 170 fs pulse is Gaussian-like but has low spectral intensity in the central lobes as shown in figure 23. Therefore, the transition probability calculated for the QD's using the experimental pulse is lower when compared to its

Gaussian counterpart. The 10 fs pulse has a non ideal shape (figure 14) and the transition probability calculated using this pulse is also lower than its Gaussian counterpart.

A comparison of the enhancement in luminescence from the experimental data and the theory was performed. The ratio of enhancement from the experiments to the enhancement from the theory using experimental pulses centered at 800 nm was 2.03. The same ratio when using 780 nm excitation for the 170 fs pulses and 800 nm excitation for the 10 fs pulse was 2.43. This data suggests that the experimental data qualitatively matched the theoretically predicted behavior.

The measured enhancement in luminescence intensity was approximately half that calculated for the QD sample. There are a number of reasons that could contribute to this discrepancy. Because the experiments were performed using two different laser systems, the beam properties (beam size, beam spatial cross-section) of the systems were different. To minimize the error due to differences in beam size, care was taken throughout the course of experiments to ensure that the beam sizes of the 170 fs and 10 fs laser were closely matched (4.5 mm diameter). Experimental error resulting from differences in focal volume and collection efficiency could also introduce errors. To minimize this, a Region of Interest (ROI) was defined in the detector array. A rectangular region was defined in X and Y direction by a start pixel, an end pixel and a group/height (binning factor). This rectangular ROI was closely matched when taking data with both the systems. The other major error could be uncompensated chirp on the broadband pulse. It has been shown that 100 fs^2 of uncompensated dispersion in the sub-10-fs pulse would result in 30 – 40% of the maximum luminescence intensity.[40] 100 fs^2

of linear chirp could be provided by ≤1 mm of glass or 4 mm of water.[40] The chirped mirrors compensate in steps of 200 fs^2. Therefore, there could also be residual second order chirp in the pulse. Interferometric autocorrelation of the compensated pulse is shown in Figure 24. This figure indicates the existence of third and higher order dispersion which is not compensated.

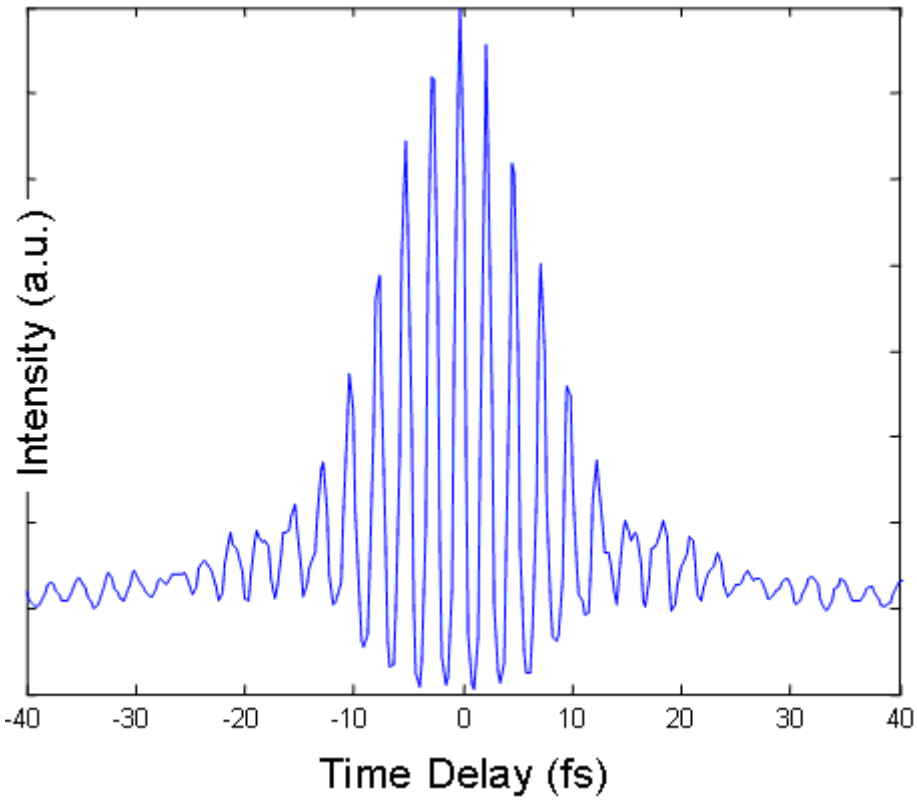

Figure 25. Autocorrelation pulsewidth of the ~10 fs pulse

The use of ultrashort pulses in NLOM systems not only enhances the luminescence signal but also facilitates spectral multiplexing. By utilizing the broad bandwidth of the ultrashort laser pulses, an array of different colored quantum dots can

more efficiently be imaged in one shot. QD's are an excellent choice for spectral multiplexing applications due to their narrow emission spectrum and broad absorption.

Comparison of pulsewidths on two photon excited luminescence from QD's does suggest that ultrashort transform limited pulses present the most efficient excitation source for a NLOM system. Nevertheless, there is a price to pay when ultrashort pulses are used. To fully appreciate the contributions from non degenerate TPA dispersion must be tightly controlled. It is however extremely difficult to maintain a 10 fs pulse at the focus and therefore difficult to achieve the full benefit of using ultrashort pulses.

FUTURE WORK

The same experiments should be repeated with a single laser system that has a center wavelength tunability and adjustable spectral bandwidth. Micra[54], a Ti: Sapphire oscillator manufactured by Coherent is a new family of compact, high-tech, broadband (>100 nm) ultrafast lasers that could be useful for future work. Typical pulse bandwidth of the Micra is shown in the figure 26. The Micra has an adjustable spectral bandwidth from less than 30 nm to over 100 nm.[54] Using Micra for the same experiments will help eliminate factors such as differences in collection efficiency and focal volume arising from variations in the beam properties.

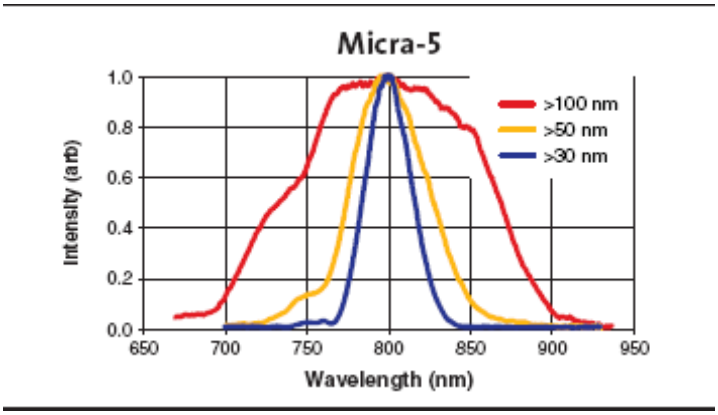

Figure 26. Possible pulsewidths using micra at 800 nm[54]

Using one system, in the experiments to evaluate the effect of transform limited pulsewidth on TPEF will yield a better comparison to the values predicted by modeling. The ultimate goal is to develop a two photon imaging system with the optimized TPE wavelength and pulsewidth. Also using biocompatible QD's as contrast agents with this systems will optimize two photon imaging.

REFERENCES

1. Smith, A. M.; Gao, X.; Nie, S., Quantum dot nanocrystals for in vivo molecular and cellular imaging. *Photochem Photobiol* **2004,** 80 (3), 377-85.

2. Loss, D.; DiVincenzo, D. P., Quantum computation with quantum dots. *Phys. Rev. A* **1998,** 57, 120 - 126.

3. Larson, D. R.; Zipfel, W. R.; Williams, R. M.; Clark, S. W.; Bruchez, M. P.; Wise, F. W.; Webb, W. W., Water-soluble quantum dots for multiphoton fluorescence imaging in vivo. *Science* **2003,** 300 (5624), 1434-6.

4. Han, M.; Gao, X.; Su, J. Z.; Nie, S., Quantum-dot-tagged microbeads for multiplexed optical coding of biomolecules. *Nat Biotechnol* **2001,** 19 (7), 631-5.

5. Stroh, M.; Zimmer, J. P.; Duda, D. G.; Levchenko, T. S.; Cohen, K. S.; Brown, E. B.; Scadden, D. T.; Torchilin, V. P.; Bawendi, M. G.; Fukumura, D.; Jain, R. K., Quantum dots spectrally distinguish multiple species within the tumor milieu in vivo. *Nat Med* **2005,** 11 (6), 678-82.

6. Jovin, T. M., Quantum dots finally come of age. *Nat Biotechnol* **2003,** 21 (1), 32-3.

7. Wu, X.; Liu, H.; Liu, J.; Haley, K. N.; Treadway, J. A.; Larson, J. P.; Ge, N.; Peale, F.; Bruchez, M. P., Immunofluorescent labeling of cancer marker Her2 and other cellular targets with semiconductor quantum dots. *Nat Biotechnol* **2003,** 21 (1), 41-6.

8. Muthukumar, S. Spectral multiplexing using quantum dot tagged microspheres with diffusing colloidal probe microscopy. Master's thesis, Texas A&M University, College Station, 2007.

9. Klimov, V. I., Nanocrystal quantum dots from fundamental photophysics to multicolor lasing. *Los Alamos Science* **2003,** 28.

10. Peyghambarian, N.; Koch, S. W.; Mysrowicz, A., *Introduction to semiconductor optics*. Prentice Hall, New Jersey, 1993.

11. Alivisatos, A. P., Semiconductor clusters, nanocrystals, and quantum dots. *Science* **1996**, 271, 933.

12. Gibbs, H. M.; Peyghambarian, N.; Khitrova, G., *Nonlinear photonics*. Springer, Berlin, 1990.

13. Quantum Dot Research - Introduction to Quantum dots. http://www.imperial.ac.uk/research/exss/research/semiconductor/qd/intro.htm (June 19, 2007).

14. Dickerson, B. D. Organometallic synthesis kinetics of CdSe quantum dots. Virginia Polytechnic Institute and State University, April 2005.

15. Snyder, C. W.; Orr, B. G.; Kessler, D.; Sander, L. M., Effect of strain on surface morphology in highly strained InGaAs films. *Physical Review Letters* **1991,** 66 (23), 3032-3035.

16. Goldstein, L.; Glas, F.; Marzin, J. Y.; Charasse, M. N.; Le Roux, G., Growth by molecular beam epitaxy and characterization of InAs/GaAs strained-layer superlattices. *Appl. Phys. Lett.* **1985**, 47, 1099.

17. B. C. Guo; Q. Pang; C. L. Yang; W. K. Ge; Yang, S. H.; Wang, J. N., In *reverse micelles synthesis and optical characterization of manganese doped CdSe quantum dots*, AIP Conference Proceedings 2005. 605-606.

18. Zhu, J.; Liao, X.; Zhao, X.; Wang, J., Photochemical synthesis and characterization of CdSe nanoparticles *Materials Letters* **2001,** 47, 339.

19. Peng, Z. A.; Peng, X., Formation of high-quality CdTe, CdSe, and CdS nanocrystals using CdO as precursor. *J Am Chem Soc* **2001,** 123 (1), 183-4.

20. Murray, C. B.; Norris, D. J.; Bawendi, M. G., Synthesis and characterization of nearly monodisperse CdE (E=S, Se, Te) semiconductor nanocrystallites. *J. Am. Chem. Soc.* **1993,** 115, 8706.

21. Murray, C. B.; Kagan, C. R.; Bawendi, M. G., Synthesis and characterization of monodisperse nanocrystals and close packed nanocrystal assemblies *Annu. Rev. Mater. Sci.* **2000,** 30, 545.

22. Herz, E. Colloidal semiconductor nanocrystals: A study of the syntheses of and capping structures for CdSe. Master's thesis, Virginia Polytechnic Institute and State University, Blacksburg 2003.

23. Hines, M. A. G.-S., P. , Synthesis and characterization of strongly luminescing ZnS-capped CdSe nanocrystals. *J. Phys. Chem.* **1996,** 100, 468-471.

24. Chan, W. C.; Nie, S., Quantum dot bioconjugates for ultrasensitive nonisotopic detection. *Science* **1998,** 281 (5385), 2016-8.

25. Saeeda Jaffar; Ki Tae Nam; Ali Khademhosseini, J. X.; Robert S. Langer; Belcher, A. M., Layer-by-layer surface modification and patterned electrostatic deposition of quantum dots. *Nano Lett* **2004,** 4 (8), 1421 -1425.

26. Smith A M, N. S., Chemical analysis and cellular imaging with quantum dots. *S. Analyst* **2004,** 129, 672.

27. Reiss, P.; Bleuse, J.; Pron, A., Highly luminescent CdSe/ZnSe core/shell nanocrystals of low size dispersion. *Nano Letters* **2002,** 2, 781.

28. Kirchner, C.; Liedl, T.; Kudera, S.; Pellegrino, T.; Javier, A. M.; Gaub, H. E.; Stolzle, S.; Fertig, N.; Parak, W. J., Cytotoxicity of colloidal CdSe and CdSe/ZnS nanoparticles. *Nano Letters* **2005,** 5, 331.

29. Derfus, A. M.; Chan, W. C. W.; Bhatia, S. N., Probing the cytotoxicity of semiconductor quantum dots *Nano Letters* **2004,** 4, 11.

30. Prasad, P. N., *Introduction to biophotonics* John Wiley & Sons, Newyork, 2004.

31. F.Kentischera; Macdonalda, R. Second harmonic generation in liquid crystals. http://moebius.physik.tu-berlin.de/lc/shg/ (June 19, 2007),

32. Goeppert-Mayer, M., Ueber elementarakte mit zwei quantenspruengen. *Ann. Phys.* **1931,** 9, 273.

33. Kaiser, W.; Garrett, C. G. B., Two-photon excitation in CaF2:Eu2+. *Phys. Rev. Lett.* **1961,** 7, 229.

34. Twarowski, A. J.; Kliger, D. S., Multiphoton absorption spectra using thermal blooming. *Chem. Phys.* **1977,** 20, 259.

35. Sheik-Bahae, M.; Said, A. A.; Wei, T.; Hagan, D.; Stryland, E. W. V., Sensitive measurement of optical nonlinearities using a single beam. *IEEE J. Quantum Electron* **1990**, (26), 760.

36. Hermann, J. P.; Ducuing, J., Absolute measurement of two-photon cross sections. *Phys. Rev. A* **1972**, (5), 2557.

37. Denk, W.; Strickler, J. H.; Webb, W. W., Two-photon laser scanning fluorescence microscopy. *Science* **1990,** 248 (4951), 73-6.

38. Tang, S.; Krasieva, T. B.; Chen, Z.; Tempea, G.; Tromberg, B. J., Effect of pulse duration on two-photon excited fluorescence and second harmonic generation in nonlinear optical microscopy. *J Biomed Opt* **2006,** 11 (2), 020501.

39. Yeh, A. T.; Larson, A. M.; Wang, C.; Pang, S.; Meissner, K. E., Two-photon absorption (and excited fluorescence) using ultrashort laser pulses. In 2007 (submitted).

40. Yeh, A. T.; Larson, A. M.; Wang, C.; Pang, S.; Meissner, K. E., Two-photon absorption (and excited fluorescence) using ultrashort laser pulses. In 2007.

41. McConnell, G., Improving the penetration depth in multiphoton excitation laser scanning microscopy. *J Biomed Opt* **2006,** 11 (5), 054020.

42. Xu, C.; Webb, W. W., Measurement of two-photon excitation cross sections of molecular fluorophores with data from 690 to 1050 nm. *Journal of the Optical Society of America B* **1996,** 13 (3), 481-491.

43. Guild, J. B.; Xu, C.; Webb, W. W., Measurement of group delay dispersion of high numerical aperture objective lenses using two-photon excited fluorescence. *Applied Optics* **1997,** 36 (1), 397-401.

44. Jasapara, J.; Rudolph, W., Characterization of sub-10-fs pulse focusing with high-numerical-aperture microscope objectives *Optics Letters* **1999,** 24 (11), 777-779.

45. Larson, A. M.; Yeh, A. T., Ex vivo characterization of sub-10-fs pulses. *Opt Lett* **2006,** 31 (11), 1681-3.

46. Denk, W.; Svoboda, K., Photon upmanship: Why multiphoton imaging is more than a gimmick. *Neuron* **1997,** 18 (3), 351-7.

47. Helmchen, F.; Denk, W., Deep tissue two-photon microscopy. *Nat Methods* **2005,** 2 (12), 932-40.

48. Multiple-photon excitation fluorescence microscopy http://www.loci.wisc.edu/multiphoton/mp.html (June 19, 2007).

49. Fundamentals and applications in multiphoton excitation microscopy. http://www.microscopyu.com/articles/fluorescence/multiphoton/multiphotonintro.html (June 19, 2007).

50. David W. Piston; Thomas J. Fellers; Davidson, M. W. Two-photon excitation in laser-scanning microscopy. http://www.microscopyu.com/articles/fluorescence/multiphoton/multiphotonintro.html (June 19, 2007).

51. Konig, K., Multiphoton microscopy in life sciences. *Journal of Microscopy* **2000,** 200, 83-104.

52. Dickerson, B. D. Organometallic synthesis kinetics of CdSe quantum dots. Ph.D dissertation, Virginia Polytechnic Institute and State University, Blacksburg, 2005.

53. Meshulach, D.; Silberberg, Y., Coherent quantum control of multiphoton transitions by shaped ultrashort optical pulses. *Physical Review A* **1999,** 60 (2), 1287-1292.

54. Micra family: Compact, broad spectral bandwidth Ti:Sapphire oscillators http://www.coherent.com/Lasers/index.cfm?fuseaction=show.page&ID=1470&loc=1470 (June 19, 2007).

VITA

Haribhaskar Balasubramanian was born in Srirangam, India. He attended school in Srirangam and Chennai, India. He received his Bachelor of Engineering degree in Electrical Engineering from the University of Mumbai in 2004. He worked as a quality assurance engineer in a pneumatics company for a year before joining Texas A&M University in August 2005. He received his Master of Science degree in Biomedical Engineering in December 2007. His mail address is 1100, Hensel Dr, Apt Y1H, College Station, TX 77840.